5 Marzano A, Gaia S, Ghisetti V *et al.* Viral load at the time of liver transplantation and risk of hepatitis B virus recurrence. *Liver Transpl* 2005; **11**: 402–9.
6 Ben-Ari Z, Daudi N, Klein A *et al.* Genotypic and phenotypic resistance: longitudinal and sequential analysis of hepatitis B virus polymerase mutations in patients with lamivudine resistance after liver transplantation. *Am J Gastroenterol* 2003; **98**: 151–9.
7 Steinmuller T, Seehofer D, Rayes N *et al.* Increasing applicability of liver transplantation for patients with hepatitis B-related liver disease. *Hepatology* 2002; **35**: 1528–35.
8 Samuel D, Muller R, Alexander G *et al.* Liver transplantation in European patients with the hepatitis B surface antigen. *N Engl J Med* 1993; **329**: 1842–7.
9 Yi N-J, Suh K-S, Cho JY *et al.* Recurrence of hepatitis B is associated with cumulative corticosteroid dose and chemotherapy against hepatocellular carcinoma recurrence after liver transplantation. *Liver Transpl* 2007; **13**: 451–8.
10 Faria LC, Gigou M, Roque-Afonso AM *et al.* Hepatocellular carcinoma is associated with an increased risk of hepatitis B virus recurrence after liver transplantation. *Gastroenterology* 2008; **134**: 1890–9; quiz 2155.
11 Saab S, Yeganeh M, Nguyen K *et al.* Recurrence of hepatocellular carcinoma and hepatitis B reinfection in hepatitis B surface antigen-positive patients after liver transplantation. *Liver Transpl* 2009; **15**: 1525–34.
12 Chun J, Kim W, Kim BG *et al.* High viremia, prolonged Lamivudine therapy and recurrent hepatocellular carcinoma predict posttransplant hepatitis B recurrence. *Am J Transplant* 2010; **10**: 1649–59.
13 Ikegami T, Soejima Y, Ohta R *et al.* Living donor liver transplantation for hepatitis B associated liver diseases: a 10-year experience in a single center. *Hepatogastroenterology* 2008; **55**: 1445–9.
14 Soejima Y, Ikegami T, Taketomi A *et al.* Hepatitis B vaccination after living donor liver transplantation. *Liver Int* 2007; **27**: 977–82.
15 Ijichi H, Yoshizumi T, Ikegami T *et al.* Recurrent hepatitis B following recurrence of hepatocellular carcinoma after living donor liver transplantation. *Fukuoka Igaku Zasshi* 2013; **104**: 376–82.
16 Soejima Y, Shimada M, Taketomi A *et al.* Successful living donor liver transplantation using a graft from a hepatitis B surface antigen-positive donor. *Liver Int* 2007; **27**: 1282–6.
17 Marzano A, Salizzoni M, Debernardi-Venon W *et al.* Prevention of hepatitis B virus recurrence after liver transplantation in cirrhotic patients treated with lamivudine and passive immunoprophylaxis. *J Hepatol* 2001; **34**: 903–10.
18 Markowitz JS, Martin P, Conrad AJ *et al.* Prophylaxis against hepatitis B recurrence following liver transplantation using combination lamivudine and hepatitis B immune globulin. *Hepatology* 1998; **28**: 585–9.
19 Ghany MG, Ayola B, Villamil FG *et al.* Hepatitis B virus S mutants in liver transplant recipients who were reinfected despite hepatitis B immune globulin prophylaxis. *Hepatology* 1998; **27**: 213–22.
20 Terrault NA, Zhou S, McCory RW *et al.* Incidence and clinical consequences of surface and polymerase gene mutations in liver transplant recipients on hepatitis B immunoglobulin. *Hepatology* 1998; **28**: 555–61.
21 Ueda Y, Marusawa H, Egawa H *et al.* De novo activation of HBV with escape mutations from hepatitis B surface antibody after living donor liver transplantation. *Antivir Ther* 2011; **16**: 479–87.
22 Gane EJ, Angus PW, Strasser S *et al.* Lamivudine plus low-dose hepatitis B immunoglobulin to prevent recurrent hepatitis B following liver transplantation. *Gastroenterology* 2007; **132**: 931–7.
23 Jiang L, Yan L, Li B *et al.* Prophylaxis against hepatitis B recurrence posttransplantation using lamivudine and individualized low-dose hepatitis B immunoglobulin. *Am J Transplant* 2010; **10**: 1861–9.
24 Fung J, Cheung C, Chan S-C *et al.* Entecavir monotherapy is effective in suppressing hepatitis B virus after liver transplantation. *Gastroenterology* 2011; **141**: 1212–9.
25 Yi N-J, Choi JY, Suh K-S *et al.* Post-transplantation sequential entecavir monotherapy following 1-year combination therapy with hepatitis B immunoglobulin. *J Gastroenterol* 2013; **48**: 1401–10.
26 Roche B, Feray C, Gigou M *et al.* HBV DNA persistence 10 years after liver transplantation despite successful anti-HBs passive immunoprophylaxis. *Hepatology* 2003; **38**: 86–95.
27 Mazzaferro V, Regalia E, Montalto F *et al.* Risk of HBV reinfection after liver transplantation in HBsAg-positive cirrhosis. Primary hepatocellular carcinoma is not a predictor for HBV recurrence. *Liver* 1996; **16**: 117–22.
28 Wong SN, Reddy KR, Keeffe EB *et al.* Comparison of clinical outcomes in chronic hepatitis B liver transplant candidates with and without hepatocellular carcinoma. *Liver Transpl* 2007; **13**: 334–42.
29 Yang H-I, Lu S-N, Liaw Y-F *et al.* Hepatitis B e antigen and the risk of hepatocellular carcinoma. *N Engl J Med* 2002; **347**: 168–74.
30 Wong PY, McPeake JR, Portmann B *et al.* Clinical course and survival after liver transplantation for hepatitis B virus infection complicated by hepatocellular carcinoma. *Am J Gastroenterol* 1995; **90**: 29–34.

Prediction of interindividual differences in hepatic functions and drug sensitivity by using human iPS-derived hepatocytes

Kazuo Takayama[a,b,c], Yuta Morisaki[a], Shuichi Kuno[a], Yasuhito Nagamoto[a,c], Kazuo Harada[d], Norihisa Furukawa[a], Manami Ohtaka[e], Ken Nishimura[f], Kazuo Imagawa[a,c,g], Fuminori Sakurai[a,h], Masashi Tachibana[a], Ryo Sumazaki[g], Emiko Noguchi[i], Mahito Nakanishi[e], Kazumasa Hirata[d], Kenji Kawabata[j,k], and Hiroyuki Mizuguchi[a,b,c,l,1]

[a]Laboratory of Biochemistry and Molecular Biology; [b]iPS Cell-based Research Project on Hepatic Toxicity and Metabolism, [d]Laboratory of Applied Environmental Biology, [h]Laboratory of Regulatory Sciences for Oligonucleotide Therapeutics, Clinical Drug Development Project, and [k]Laboratory of Biomedical Innovation, Graduate School of Pharmaceutical Sciences, Osaka University, Osaka 565-0871, Japan; [c]Laboratory of Hepatocyte Regulation, and [j]Laboratory of Stem Cell Regulation, National Institute of Biomedical Innovation, Osaka 567-0085, Japan; [e]Research Center for Stem Cell Engineering, National Institute of Advanced Industrial Science and Technology, Ibaraki 305-8562, Japan; [f]Laboratory of Gene Regulation, [g]Department of Child Health, and [i]Department of Medical Genetics, Faculty of Medicine, University of Tsukuba, Ibaraki 305-8575, Japan; and [l]The Center for Advanced Medical Engineering and Informatics, Osaka University, Osaka 565-0871, Japan

Edited by Shinya Yamanaka, Kyoto University, Kyoto, Japan, and approved October 17, 2014 (received for review July 16, 2014)

Interindividual differences in hepatic metabolism, which are mainly due to genetic polymorphism in its gene, have a large influence on individual drug efficacy and adverse reaction. Hepatocyte-like cells (HLCs) differentiated from human induced pluripotent stem (iPS) cells have the potential to predict interindividual differences in drug metabolism capacity and drug response. However, it remains uncertain whether human iPSC-derived HLCs can reproduce the interindividual difference in hepatic metabolism and drug response. We found that cytochrome P450 (CYP) metabolism capacity and drug responsiveness of the primary human hepatocytes (PHH)-iPS-HLCs were highly correlated with those of PHHs, suggesting that the PHH-iPS-HLCs retained donor-specific CYP metabolism capacity and drug responsiveness. We also demonstrated that the interindividual differences, which are due to the diversity of individual SNPs in the CYP gene, could also be reproduced in PHH-iPS-HLCs. We succeeded in establishing, to our knowledge, the first PHH-iPS-HLC panel that reflects the interindividual differences of hepatic drug-metabolizing capacity and drug responsiveness.

human iPS cells | hepatocyte | CYP2D6 | personalized drug therapy | SNP

Drug-induced liver injury (DILI) is a leading cause of the withdrawal of drugs from the market. Human induced pluripotent stem cell (iPSC)-derived hepatocyte-like cells (HLCs) are expected to be useful for the prediction of DILI in the early phase of drug development. Many groups, including our own, have reported that the human iPS-HLCs have the ability to metabolize drugs, and thus these cells could be used to detect the cytotoxicity of drugs that are known to cause DILI (1, 2). However, to accurately predict DILI, it will be necessary to establish a panel of human iPS-HLCs that better represents the genetic variation of the human population because there are large interindividual differences in the drug metabolism capacity and drug responsiveness of hepatocytes (3). However, it remains unclear whether the drug metabolism capacity and drug responsiveness of human iPS-HLCs could reflect those of donor parental primary human hepatocytes (PHHs). To address this issue, we generated the HLCs differentiated from human iPSCs which had been established from PHHs (PHH-iPS-HLCs). Then, we compared the drug metabolism capacity and drug responsiveness of PHH-iPS-HLCs with those of their parental PHHs, which are genetically identical to the PHH-iPS-HLCs.

Interindividual differences of cytochrome P450 (CYP) metabolism capacity are closely related to genetic polymorphisms, especially single nucleotide polymorphisms (SNPs), in CYP genes (4). Among the various CYPs expressed in the liver, CYP2D6 is responsible for the metabolism of approximately a quarter of commercially used drugs and has the largest phenotypic variability, largely due to SNPs (5). It is known that certain alleles result in the poor metabolizer phenotype due to a decrease of CYP2D6 metabolism. Therefore, the appropriate dosage for drugs that are metabolized by CYP2D6, such as tamoxifen, varies widely among individuals (6). Indeed, in the 1980s, polymorphism in CYP2D6 appears to have contributed to the withdrawal of CYP2D6-metabolized drugs such as perhexiline from the market in many countries (7). If we could establish a panel of HLCs that better represents the diversity of genetic polymorphisms in the human population, it might be possible to determine the appropriate dosage of a drug for a particular individual. However, it is not known whether the drug metabolism capacity and drug responsiveness of HLCs reflect the genetic diversity, including SNPs, in CYP genes. Therefore, in this study we generated HLCs from several PHHs that have various SNPs on CYP2D6 and then compared the CYP2D6 metabolism capacity and responses to CYP2D6-metabolized drugs between the PHH-iPS-HLCs and parental PHHs.

Significance

We found that individual cytochrome P450 (CYP) metabolism capacity and drug sensitivity could be predicted by examining them in the primary human hepatocytes–human induced pluripotent stem cells–hepatocyte-like cells (PHH-iPS-HLCs). We also confirmed that interindividual differences of CYP metabolism capacity and drug responsiveness that are due to the diversity of individual single nucleotide polymorphisms in the CYP gene could also be reproduced in the PHH-iPS-HLCs. These findings suggest that interindividual differences in drug metabolism capacity and drug response could be predicted by using HLCs differentiated from human iPS cells. We believe that iPS-HLCs would be a powerful technology not only for accurate and efficient drug development, but also for personalized drug therapy.

Author contributions: K.T. and H.M. designed research; K.T., Y.M., and S.K. performed research; K.T., Y.M., Kazuo Harada, M.O., K.N., K.I., M.N., and Kazumasa Hirata contributed new reagents/analytic tools; K.T., Y.N., N.F., F.S., M.T., R.S., E.N., K.K., and H.M. analyzed data; and K.T. and H.M. wrote the paper.

The authors declare no conflict of interest.

This article is a PNAS Direct Submission.

Data deposition: The DNA microarray data reported in this paper have been deposited in the Gene Expression Omnibus (GEO) database, www.ncbi.nlm.nih.gov/geo (accession no. GSE61287).

[1]To whom correspondence should be addressed. Email: mizuguch@phs.osaka-u.ac.jp.

This article contains supporting information online at www.pnas.org/lookup/suppl/doi:10.1073/pnas.1413481111/-/DCSupplemental.

To this end, PHHs were reprogrammed into human iPSCs and then differentiated into the HLCs. To examine whether the HLCs could reproduce the characteristics of donor PHHs, we first compared the CYP metabolism capacity and response to a hepatotoxic drug between PHHs and genetically identical PHH-iPS-HLCs (12 donors were used in this study). Next, analyses of hepatic functions, including comparisons of the gene expression of liver-specific genes and CYPs, were performed to examine whether the hepatic characteristics of PHHs were reproduced in the HLCs. To the best of our knowledge, this is the first study to compare the functions between iPSC-derived cells from various donors and their parental cells with identical genetic backgrounds. Finally, we examined whether the PHH-iPS-HLCs exhibited a capacity for drug metabolism and drug responsiveness that reflect the genetic diversity such as SNPs on CYP genes.

Results

Reprogramming of PHHs to Human iPSCs. To examine whether the HLCs could reproduce interindividual differences in liver functions, we first tried to generate human iPSCs from the PHHs of 12 donors. PHHs were transduced with a Yamanaka 4 factor-expressing SeV (SeVdp-iPS) vector (*SI Appendix*, Fig. S1*A*) in the presence of SB431542, PD0325901, and a rock inhibitor, which could promote the somatic reprogramming (8). The reprogramming procedure is shown in *SI Appendix*, Fig. S1*B*. The human iPSCs generated from PHHs (PHH-iPSCs) were positive for alkaline phosphatase (*SI Appendix*, Fig. S1*B*, *Right*), NANOG, OCT4, SSEA4, SOX2, Tra1-81, and KLF4 (Fig. 1*A*). The gene expression levels of the pluripotent markers (*OCT3/4*, *SOX2*, and *NANOG*) in the PHH-iPSCs were approximately equal to those in human embryonic stem cells (ESCs) (*SI Appendix*, Fig. S1*C*, *Left*). The gene expression levels of the hepatic markers [*albumin (ALB)*, *CYP3A4*, and *αAT*] in the PHH-iPSCs were significantly lower than those in the parental PHHs (*SI Appendix*, Fig. S1*C*, *Right*). We also confirmed that the PHH-iPSCs have the ability to differentiate into the three embryonic germ layers in vitro by embryoid body formation and in vivo by teratoma formation (*SI Appendix*, Fig. S2 *A* and *B*, respectively). To verify that the PHH-iPSCs originated from PHHs, short tandem repeat analysis was performed in the PHH-iPSCs and parental PHHs (*SI Appendix*, Fig. S2*C*). The results showed that the PHH-iPSCs were indeed originated from PHHs. Taken together, these results indicated that the generation of human iPSCs from PHHs was successfully performed. It is known that a transient epigenetic memory of the original cells is retained in early-passage iPSCs, but not in late-passage iPSCs (9). To examine whether the hepatic differentiation capacity of PHH-iPSCs depends on their passage number, PHH-iPSCs having various passage numbers were differentiated into the hepatic lineage (Fig. 1*B*). The *tyrosine aminotransferase* (*TAT*) expression levels and albumin (ALB) secretion levels in early passage PHH-iPS-HLCs (fewer than 10 passages) were higher than those of late passage PHH-iPS-HLCs (more than 14 passages). These results suggest that the hepatic differentiation tendency is maintained in early passage PHH-iPSCs, but not in late passage PHH-iPSCs. In addition, the hepatic functions of late passage PHH-iPS-HLCs were similar to those in the HLCs derived from late passage non–PHH-derived iPS cells (such as dermal cells, blood cells, and Human Umbilical Vein Endothelial Cells (HUVEC)-derived iPS cells) (*SI Appendix*, Fig. S3). Therefore, PHH-iPSCs, which were passaged more than 20 times, were used in our study to avoid any potential effect of transient epigenetic memory retained in parental PHHs on hepatic functions.

HLCs Were Differentiated from PHH-iPSCs Independent of Their Differentiation Tendency. To compare the hepatic characteristics among the PHH-iPS-HLCs that were generated from PHHs of the 12 donors, all of the PHH-iPSCs were differentiated into the HLCs as described in Fig. 2*A*. However, the differences in hepatic function among PHH-iPS-HLCs could not be properly compared because there were large inter-PHH-iPSC line differences in the hepatic differentiation efficiency based on ALB or asialoglycoprotein receptor 1 (ASGR1) expression analysis (Fig. 2*B*). In addition, there were also large inter-PHH-iPS-HLC line differences in ALB or urea secretion capacities (Fig. 2*C*). These results suggest that it is impossible to compare the hepatic characteristics among PHH-iPS-HLCs without compensating for the differences in the hepatic differentiation efficiency. Recently, we developed a method to maintain and proliferate the hepatoblast-like cells (HBCs) generated from human ESCs/iPSCs by using human laminin 111 (LN111) (10). To examine whether the hepatic differentiation efficiency could be made uniform by generating the HLCs following purification and proliferation of the HBCs, the PHH-iPS-HBCs were cultured on LN111 as

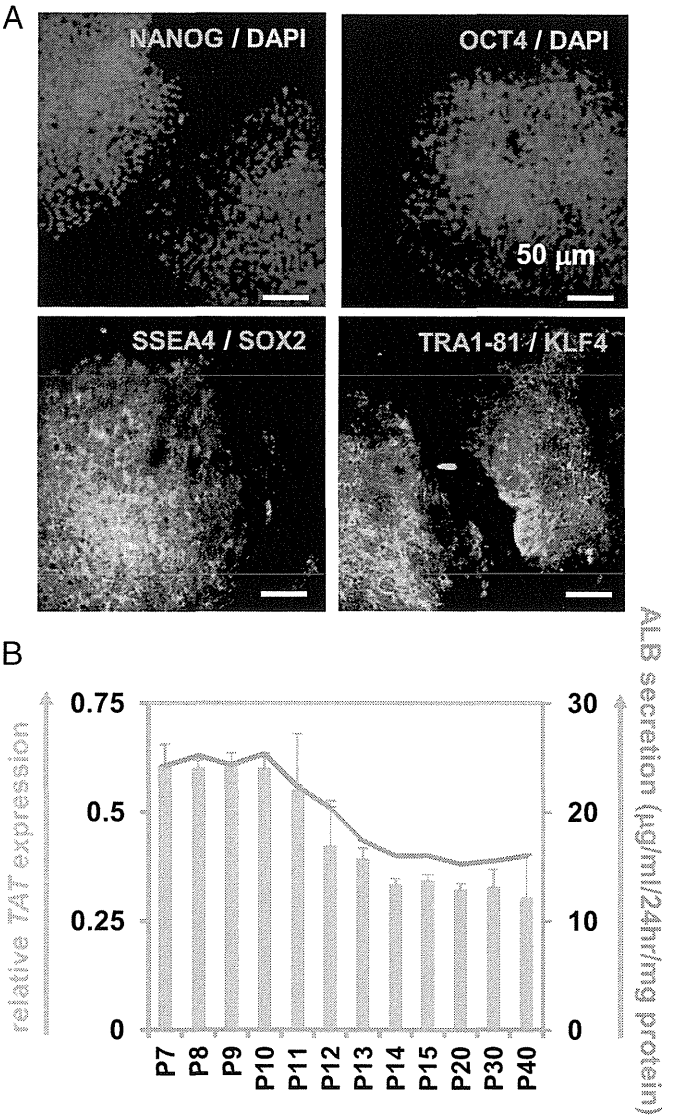

Fig. 1. Establishment and characterization of human iPSCs generated from PHHs. (*A*) The PHH-iPSCs were subjected to immunostaining with anti-NANOG (red), OCT4 (red), SSEA4 (green), SOX2 (red), TRA1-81 (green), and KLF4 (red) antibodies. Nuclei were counterstained with DAPI (blue) (*Upper*). (*B*) The *TAT* expression and ALB secretion levels in the PHH-iPS-HLCs (P7–P40) were examined. On the *y* axis, the gene expression level of *TAT* in PHHs was taken as 1.0.

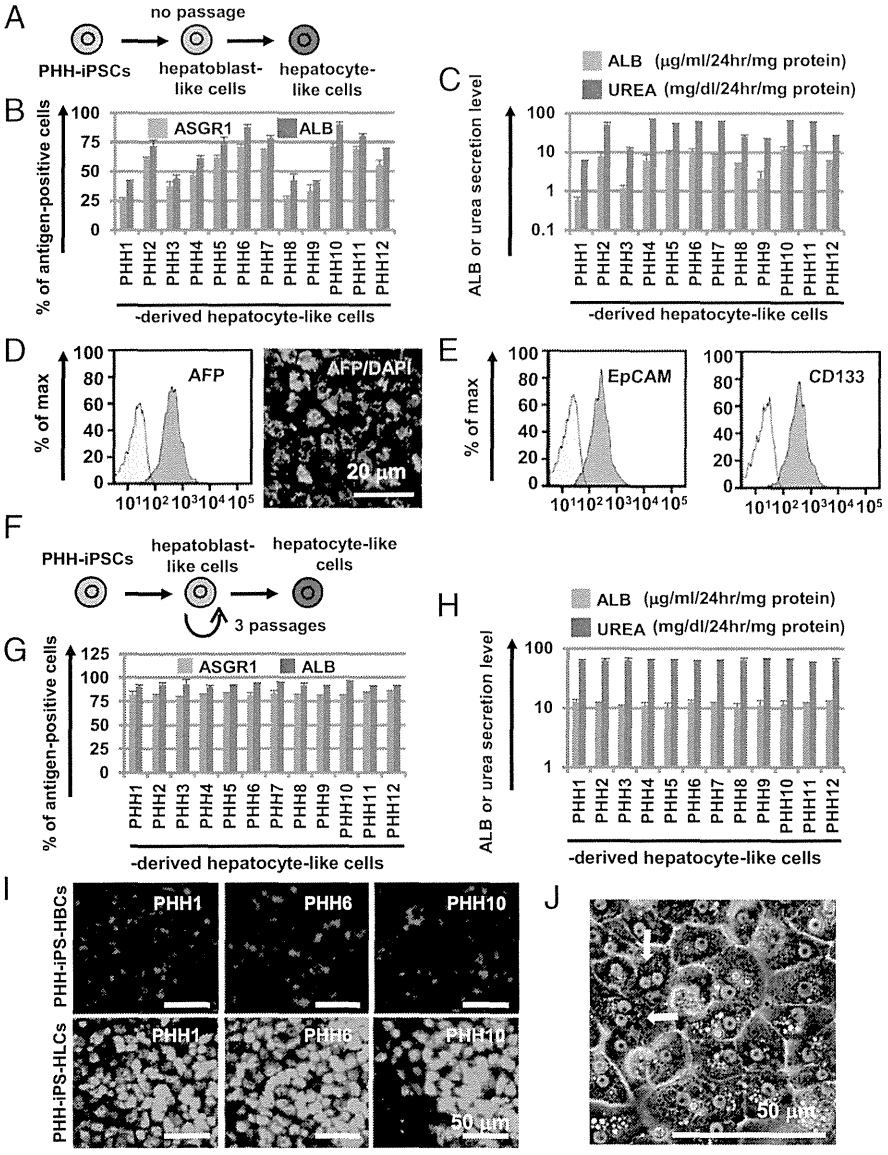

Fig. 2. Highly efficient hepatocyte differentiation from PHH-iPSCs independent of their differentiation tendency. (*A*) PHH-iPSCs were differentiated into the HLCs via the HBCs. (*B*) On day 25 of differentiation, the efficiency of hepatocyte differentiation was measured by estimating the percentage of ASGR1- or ALB-positive cells using FACS analysis. (*C*) The amount of ALB or urea secretion was examined in PHH-iPS-HLCs. (*D*) The percentage of AFP-positive cells in PHH-iPS-HBCs was examined by using FACS analysis (*Left*). The PHH-iPS-HBCs were subjected to immunostaining with anti-AFP (green) antibodies. Nuclei were counterstained with DAPI (blue) (*Right*). (*E*) The percentage of EpCAM- and CD133-positive cells in PHH-iPS-HBCs was examined by using FACS analysis (*Left*). (*F*) PHH-iPSCs were differentiated into the hepatic lineage, and then PHH-iPS-HBCs were purified and maintained for three passages on human LN111. Thereafter, expanded PHH-iPS-HBCs were differentiated into the HLCs. (*G*) The efficiency of hepatic differentiation from PHH-iPS-HBCs was measured by estimating the percentage of ASGR1- or ALB-positive cells using FACS analysis. (*H*) The amount of ALB or urea secretion in PHH-iPS-HLCs was examined. Data represent the mean ± SD from three independent differentiations. (*I*) The PHH1-, 6-, or 10-iPS-HBCs and -HLCs were subjected to immunostaining with anti-αAT (green) antibodies. Nuclei were counterstained with DAPI (blue). (*J*) A phase-contrast micrograph of PHH-iPS-HLCs.

previously described (10), and then differentiated into the HLCs. Almost all of the cells were positive for the hepatoblast marker [alpha-fetoprotein (AFP)] (Fig. 2*D*). In addition, the PHH-iPS-HBCs were positive for two other hepatoblast markers, EpCAM and CD133 (Fig. 2*E*). To examine the hepatic differentiation efficiency of the PHH-iPS-HBCs maintained on LN111-coated dishes for three passages (Fig. 2*F*), the HBCs were differentiated into the HLCs, and then the percentage of ALB- and ASGR1-positive cells was measured by FACS analysis (Fig. 2*G*). All 12 PHH-iPS-HBCs could efficiently differentiate into the HLCs, yielding more than 75% or 85% ASGR1- or ALB-positive cells, respectively. In addition, there was little difference between the PHH-iPSC lines in ALB or urea secretion capacities (Fig. 2*H*). Although there were large differences in the hepatic differentiation capacity among the PHH1/6/10 (Fig. 2*B*), PHH1/6/10-iPS-HBCs could efficiently differentiate into the HLCs that homogeneously expressed αAT (Fig. 2*I*). After the hepatic differentiation of the PHH-iPS-HBCs, the morphology of the HLCs was similar to that of the PHHs: polygonal with distinct round binuclei (Fig. 2*J*). These results indicated that the hepatic differentiation efficiency of the 12 PHH-iPSC lines could be rendered uniform by inducing hepatic maturation after the establishment of self-renewing HBCs. Therefore, we expected that differences in the hepatic characteristics among the HLCs generated from the 12 individual donor PHH-iPS-HBCs could be properly compared. In addition, the hepatic differentiation efficiency could be rendered uniform not only in the PHH-iPSC lines but also in non–PHH-iPSC lines and human ESCs by performing hepatic maturation after the establishment of self-renewing HBCs (*SI Appendix*, Fig. S4). In Figs. 3 and 4, the HLCs were differentiated after the HBC proliferation step to normalize the hepatic differentiation efficiency.

PHH-iPS-HLCs Retained Donor-Specific Drug Metabolism Capacity and Drug Responsiveness. To examine whether the hepatic functions of individual PHH-iPS-HLCs reflect those of individual PHHs, the CYP metabolism capacity and drug responsiveness of PHH-iPS-HLCs were compared with those of PHHs. PHHs are often used as a positive control to assess the hepatic functions of the HLCs, although in all of the previous reports, the donor of PHHs has been different from that of human iPSCs. Because it is generally considered that CYP activity differs widely among individuals, the hepatic functions of the HLCs should be compared with those of genetically identical PHHs to accurately evaluate the hepatic functions of the HLCs. The CYP1A2, -2C9, and -3A4 activity levels in the PHH-iPS-HLCs were ~60% of

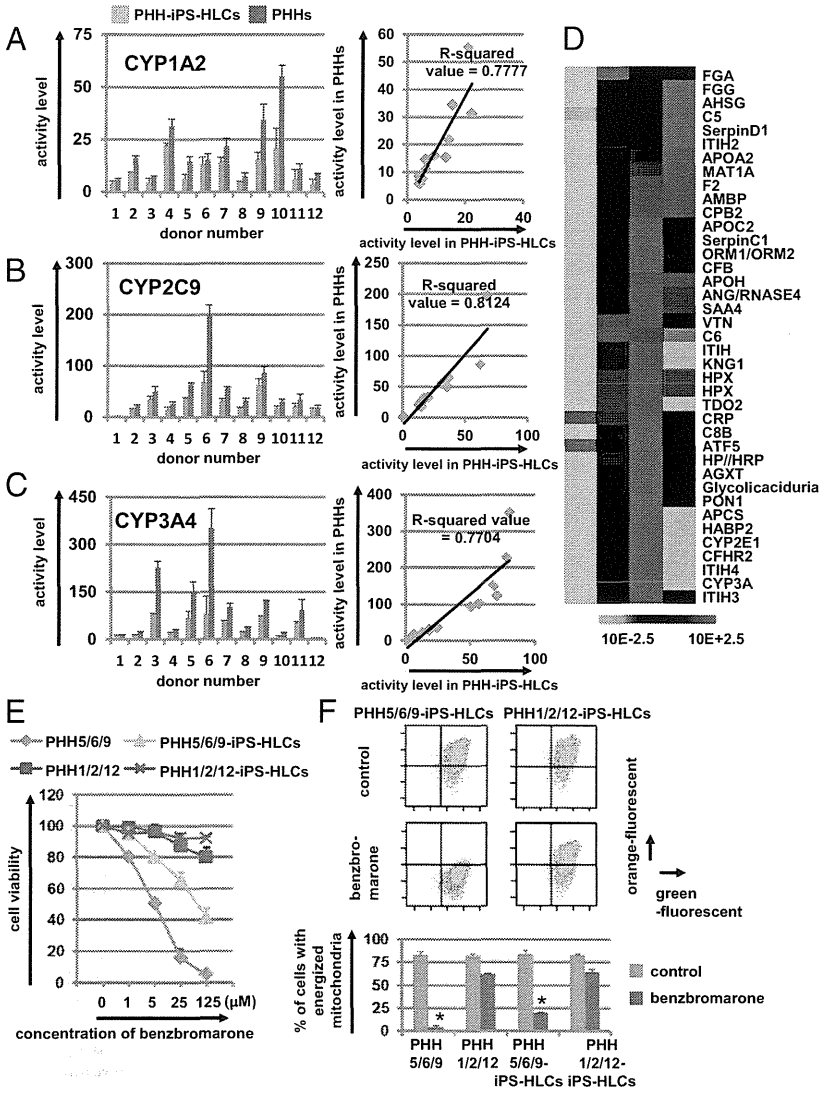

Fig. 3. The drug metabolism capacity and drug responsiveness of PHH-iPS-HLCs were highly correlated with those of their parental PHHs. (*A–C*) CYP1A2 (*A*), -2C9 (*B*), and -3A4 (*C*) activity levels in PHH-iPS-HLCs and PHHs were measured by LC-MS/MS analysis. The R-squared values are indicated in each figure. (*D*) The global gene expression analysis was performed in PHH9-iPSCs, PHH9-iPS-HLCs, PHH9s, and HepG2 (PHH-iPSCs, PHH-iPS-HLCs, and PHHs are genetically identical). Heat-map analyses of liver-specific genes are shown. (*E*) The cell viability of PHH5/6/9, PHH1/2/12, PHH5/6/9-iPS-HLCs, and PHH1/2/12-iPS-HLCs was examined after 24 h exposure to different concentrations of benzbromarone. The cell viability was expressed as a percentage of that in the cells treated only with solvent. (*F*) The percentage of cells with energized mitochondria in the DMSO-treated (control, *Upper*) or benzbromarone-treated (*Lower*) cells based on FACS analysis. Double-positive cells (green+/orange+) represent energized cells, whereas single-positive cells (green+/orange–) represent apoptotic and necrotic cells. Data represent the mean ± SD from three independent experiments (*Lower Graph*). Student *t* test indicated that the percentages in the "control" were significantly higher than those in the "benzbromarone" group ($P < 0.01$). The "PHH5/6/9" represents the average value of cell viability (*E*) or mitochondrial membrane potential (*F*) in PHH5, PHH6, and PHH9. The "PHH1/2/12" represents the average value of cell viability or mitochondrial membrane potential in PHH1, PHH2, and PHH12. PHH5, PHH6, and PHH9 were the top three with respect to CYP2C9 activity levels, whereas PHH1, PHH2, and PHH12 had the lowest CYP2C9 activity levels.

those in the PHHs (Fig. 3 *A–C* and *SI Appendix*, Fig. S5). Interestingly, the CYP1A2, -2C9, and -3A4 activity levels in the PHH-iPS-HLCs were highly correlated with those in the PHHs (the R-squared values were more than 0.77) (Fig. 3 *A*, *B*, and *C*, respectively). These results suggest that it would be possible to predict the individual CYP activity levels through analysis of the CYP activity levels of the PHH-iPS-HLCs. Because the average and variance of CYP3A4 activity levels in PHH-iPS-HLCs, non–PHH-iPS-HLCs, and human ES-HLCs were similar to each other (*SI Appendix*, Fig. S6), the drug metabolism capacity of PHH-iPS-HLCs might be similar to that of nonliver tissue-derived iPS-HLCs and human ES-HLCs. Therefore, it might be possible to predict the diversity of drug metabolism capacity among donors by using nonliver tissue-derived iPS-HLCs and human ES-HLCs as well as PHH-iPS-HLCs. On the other hand, the CYP induction capacities of PHH-iPS-HLCs were weakly correlated with those of PHHs (*SI Appendix*, Fig. S7 *A–C*). To further investigate the characteristics of the HLCs, DNA microarray analyses were performed in genetically identical undifferentiated iPSCs, PHH-iPS-HLCs, and PHHs. The gene expression patterns of liver-specific genes, CYPs, and transporters in the PHH-iPS-HLCs were similar to those in PHHs (Fig. 3*D* and *SI Appendix*, Fig. S7 *D* and *E*, respectively). Next, the hepatotoxic drug responsiveness of PHH-iPS-HLCs was compared with that of PHHs. Benzbromarone, which is known to cause hepatotoxicity by CYP2C9 metabolism (11), was treated to PHH5/6/9 and PHH5/6/9-iPS-HLCs, which have high CYP2C9 activity, or PHH1/2/12 and PHH1/2/12-iPS-HLCs which have low CYP2C9 activity (Fig. 3*E*). The susceptibility of the PHH5/6/9 and PHH5/6/9-iPS-HLCs to benzbromarone was higher than that of PHH1/2/12 and PHH1/2/12-iPS-HLCs, respectively. These results were attributed to the higher CYP2C9 activity levels in PHH5/6/9 and PHH5/6/9-iPS-HLCs compared with those in PHH1/2/12 and PHH1/2/12-iPS-HLCs. Because it is also known that benzbromarone causes mitochondrial toxicity (12), an assay of mitochondrial membrane potential was performed in benzbromarone-treated PHHs and PHH-iPS-HLCs (Fig. 3*F*). The mitochondrial toxicity observed in PHH5/6/9 and PHH5/6/9-iPS-HLCs was more severe than that in PHH1/2/12 and PHH1/2/12-iPS-HLCs, respectively. Taken together, these results suggest that the hepatic functions of the individual PHH-iPS-HLCs were highly correlated with those of individual PHHs.

Interindividual Differences in CYP2D6-Mediated Metabolism and Drug Toxicity, Which Are Caused by SNPs in CYP2D6, Are Reproduced in the PHH-iPS-HLCs. Because certain SNPs are known to have a large impact on CYP activity, the genetic variability of CYP plays an important role in interindividual differences in drug response. CYP2D6 shows the large phenotypic variability due to genetic polymorphism (13). We next examined whether the PHHs used

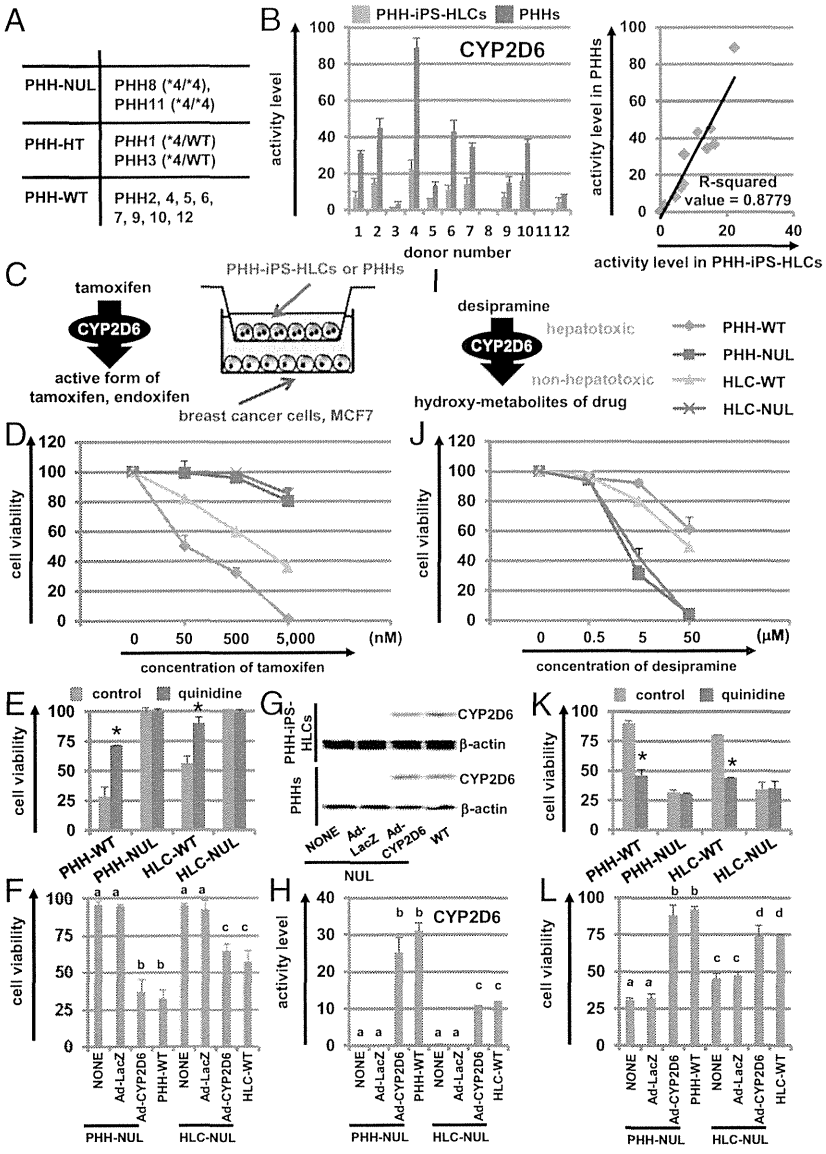

Fig. 4. The interindividual differences in CYP2D6 metabolism capacity and drug responsiveness induced by SNPs in CYP2D6 are reproduced in the PHH-iPS-HLCs. (*A*) SNPs (CYP2D6*3, *4, *5, *6, *7, *8, *16, and *21) in the CYP2D6 gene were analyzed. (*B*) The CYP2D6 activity levels in PHH-iPS-HLCs and PHHs were measured by LC-MS/MS analysis. (*C*) The pharmacological activity of tamoxifen-dependent conversion to its metabolite, endoxifen, by the CYP2D6. The coculture system of breast cancer cells (MCF-7 cells) and the PHH-iPS-HLCs are illustrated. (*D*) The cell viability of MCF-7 cells was assessed after 72-h exposure to different concentrations of tamoxifen. (*E*) The cell viability of MCF-7 cells, which were cocultured with PHH-WT, PHH-NUL, HLC-WT, and HLC-NUL, was assessed after 72-h exposure to 500 nM of tamoxifen in the presence or absence of 3 nM quinidine (a CYP2D6 inhibitor). (*F*) The cell viability of MCF-7 cells cocultured with Ad-CYP2D6-transduced PHH-NUL and HLC-NUL was examined after 72-h exposure to 500 nM of tamoxifen. (*G* and *H*) The CYP2D6 expression (*G*) and activity (*H*) levels in Ad-CYP2D6-transduced PHH-NUL and HLC-NUL were examined by Western blotting and LC-MS/MS analysis. (*I*) The detoxification of desipramine-dependent conversion to its conjugated form by the CYP2D6. (*J*) The cell viability of PHH-WT, PHH-NUL, HLC-WT, and HLC-NUL was assessed after 24-h exposure to different concentrations of desipramine. (*K*) The cell viability of the PHH-WT and HLC-WT was assessed after 24-h exposure to 5 μM of desipramine in the presence or absence of 5 μM of quinidine (a CYP2D6 inhibitor). (*L*) The cell viability of the Ad-CYP2D6-transduced PHH-NUL and HLC-NUL was examined after 24-h exposure to 5 μM of desipramine. The cell viability was expressed as a percentage of that in the cells treated with only solvent. Data represent the mean ± SD from three independent experiments. In *E* and *K*, Student *t* test indicated that the cell viability in the "control" was significantly higher than that in the "quinidine" group ($P < 0.01$). In *F*, *H*, and *L*, statistical significance was evaluated by ANOVA followed by Bonferroni post hoc tests to compare all groups. Groups that do not share the same letter are significantly different from each other ($P < 0.05$).

in this study have the CYP2D6 poor metabolizer genotypes (CYP2D6 *3, *4, *5, *6, *7, *8, *16, and *21) (5). PHH8 and -11 have CYP2D6*4 (null allele), whereas the others have a wild type (WT) or hetero allele (*SI Appendix*, Table S3 and Fig. 4*A*). Consistent with this finding, the PHH8/11-iPS-HLCs also have CYP2D6*4, whereas the others have a wild type or hetero allele. As expected, the CYP2D6 activity levels in the PHH8/11 (PHH-NUL) and PHH8/11-iPS-HLC (HLC-NUL) were significantly lower than those in the PHH-WT and HLC-WT, respectively (Fig. 4*B*). The pharmacological activity of tamoxifen, which is the most widely used agent for patients with breast cancer, is dependent on its conversion to its metabolite, endoxifen, by the CYP2D6 (Fig. 4*C*). To examine whether the pharmacological activity of tamoxifen could be predicted by using PHHs and HLCs that have either the null type CYP2D6*4 allele or wild-type CYP2D6 allele, the breast cancer cell line MCF7 was cocultured with PHHs or HLCs, and then the cells were treated with tamoxifen (Fig. 4*D*). The cell viability of MCF7 cells cocultured with PHHs-NUL or HLCs-NUL was significantly higher than that of MCF7 cells cocultured with PHHs-WT or HLCs-WT. The decrease in cell viability of MCF7 cells cocultured with PHHs-WT or HLCs-WT was rescued by treatment with a CYP2D6 inhibitor, quinidine (Fig. 4*E*). We also confirmed that the cell viability of MCF7 cells cocultured with PHHs-NUL or HLCs-NUL was decreased by CYP2D6 overexpression in the PHHs-NUL or HLCs-NUL (Fig. 4*F*). Note that the expression (Fig. 4*G*) and activity (Fig. 4*H*) levels of CYP2D6 in CYP2D6-expressing adenovirus vector (Ad-CYP2D6)-transduced PHHs-NUL or HLCs-NUL were comparable to those of PHHs-WT or HLCs-WT. These results indicated that the PHHs-WT and HLCs-WT could more efficiently metabolize tamoxifen than the PHHs-NUL and HLCs-NUL, respectively, and thereby induced higher toxicity in MCF7 cells. Similar results were obtained with the other breast cancer cell line, T-47D (*SI Appendix*, Fig. S8 *A*–*D*). Next, we examined whether the CYP2D6-mediated drug-induced hepatotoxicity could be predicted by using PHHs and HLCs having either a null type CYP2D6*4 allele or wild-type CYP2D6 allele. PHHs and HLCs were treated with desipramine, which is known to cause hepatotoxicity (Fig. 4*I*) (14). The cell viability of PHHs-NUL and HLCs-NUL was significantly lower than that of PHHs-WT and HLCs-WT (Fig. 4*J*). The cell viability of the PHHs-WT or HLCs-WT was decreased by treatment with a CYP2D6 inhibitor, quinidine (Fig. 4*K*). We also confirmed that the decrease in the cell viability of the PHHs-NUL or HLCs-NUL was rescued by CYP2D6 overexpression in the PHHs-NUL or HLCs-NUL (Fig. 4*L*). Similar

results were obtained with the other hepatotoxic drug, perhexiline (*SI Appendix*, Fig. S8 *E–H*). These results indicated that the PHHs-WT and HLCs-WT could more efficiently metabolize imipramine and thereby reduce toxicity compared with the PHHs-NUL and HLCs-NUL. Taken together, our findings showed that the interindividual differences in CYP metabolism capacity and drug responsiveness, which are prescribed by an SNP in genes encoding CYPs, were also reproduced in the PHH-iPS-HLCs.

Discussion

The purpose of this study was to examine whether the individual HLCs could reproduce the hepatic function of individual PHHs. A Yamanaka 4 factor-expressing SeV vector was used in this study to generate integration-free human iPSCs from PHHs. It is known that SeV vectors can express exogenous genes without chromosomal insertion, because these vectors replicate their genomes exclusively in the cytoplasm (15). To examine the different cellular phenotypes associated with SNPs in human iPSC derivatives, the use of integration-free human iPSCs is essential.

We found that the CYP activity levels of the PHH-iPS-HLCs reflected those of parent PHHs, as shown in Fig. 3 *A–C*. There were few interindividual differences in the ratio of CYP expression levels in the PHH-iPS-HLCs to those in PHHs (*SI Appendix*, Fig. S5). Together, these results suggest that it is possible to predict the individual CYP activity levels through analysis of the CYP activity levels of the PHH-iPS-HLCs. In the future, it will be necessary to confirm these results in skin or blood cell-derived iPSCs as well as PHH-iPSCs, although donor-matched PHHs and blood cells (or skin cells) are difficult to obtain. In addition, the comparison of hepatic functions between genetically identical PHHs and PHH-iPS-HLCs (Fig. 3 *A–C*) would enable us to accurately ascertain whether the HLCs exhibit sufficient hepatic function to be a suitable substitute for PHHs in the early phase of pharmaceutical development. Because the drug responsiveness of the individual HLCs reflected that of individual PHHs (Fig. 3 *E* and *F*), it might be possible to perform personalized drug therapy following drug screening using a patient's HLCs. However, the R-squared values of the individual CYP activities differed from each other (Fig. 3 *A–C*), suggesting that the activity levels of some CYPs are largely influenced not only by genetic information but also by environmental factors, such as dietary or smoking habits.

The interindividual differences of CYP2D6 metabolism capacity and drug responsiveness that were prescribed by SNP in genes encoding CYP2D6 were reproduced in the PHH-iPS-HLCs (Fig. 4). It was impossible to perform drug screening in the human hepatocytes derived from a donor with rare SNPs because these hepatocytes could not be obtained. However, because human iPSCs can be generated from such donors with rare SNPs, the CYP metabolism capacity and drug responsiveness of these donors might be possible to predict. Further, it would also be possible to identify the novel SNP responsible for an unexpected hepatotoxicity by using the HLCs in which whole genome sequences are known. We thus believe that the HLCs will be a powerful tool not only for accurate and efficient drug development but also for personalized drug therapy.

Experimental Procedures

DNA Microarray. Total RNA was prepared from the PHH9-iPSCs, PHH9-iPS-HLCs, PHH9, and human hepatocellular carcinoma cell lines by using an RNeasy Mini kit. A pool of three independent samples was used in this study. cRNA amplifying, labeling, hybridizing, and analyzing were performed at Miltenyi Biotec. The Gene Expression Omnibus (GEO) accession no. for the microarray analysis is GSE61287.

Flow Cytometry. Single-cell suspensions of human iPSC-derived cells were fixed with 2% (vol/vol) paraformaldehyde (PFA) for 20 min, and then incubated with the primary antibody (described in *SI Appendix*, Table S1), followed by the secondary antibody (described in *SI Appendix*, Table S2). In case of the intracellular staining, the Permeabilization Buffer (eBioscience) was used to create holes in the membrane thereby allowing the antibodies to enter the cell effectively. Flow cytometry analysis was performed using a FACS LSR Fortessa flow cytometer (BD Biosciences).

ACKNOWLEDGMENTS. We thank Yasuko Hagihara, Natsumi Mimura, and Shigemi Isoyama for their excellent technical support. H.M. and K.K. were supported by grants from the Ministry of Health, Labor, and Welfare. H.M. was also supported by the Project for Technological Development, Research Center Network for Realization of Regenerative Medicine of the Japan Science and Technology Agency and by the Uehara Memorial Foundation. F.S. was supported by the Program for Promotion of Fundamental Studies in Health Sciences of the National Institute of Biomedical Innovation. K.T. and Y.N. were supported by a grant-in-aid for the Japan Society for the Promotion of Science Fellows.

1. Takayama K, et al. (2012) Efficient generation of functional hepatocytes from human embryonic stem cells and induced pluripotent stem cells by HNF4α transduction. *Mol Ther* 20(1):127–137.
2. Medine CN, et al. (2013) Developing high-fidelity hepatotoxicity models from pluripotent stem cells. *Stem Cells Transl Med* 2(7):505–509.
3. Ingelman-Sundberg M (2004) Pharmacogenetics of cytochrome P450 and its applications in drug therapy: The past, present and future. *Trends Pharmacol Sci* 25(4): 193–200.
4. Ingelman-Sundberg M (2001) Genetic susceptibility to adverse effects of drugs and environmental toxicants. The role of the CYP family of enzymes. *Mutat Res* 482(1-2): 11–19.
5. Zhou SF (2009) Polymorphism of human cytochrome P450 2D6 and its clinical significance: Part I. *Clin Pharmacokinet* 48(11):689–723.
6. Borges S, et al. (2006) Quantitative effect of CYP2D6 genotype and inhibitors on tamoxifen metabolism: Implication for optimization of breast cancer treatment. *Clin Pharmacol Ther* 80(1):61–74.
7. Bakke OM, Manocchia M, de Abajo F, Kaitin KI, Lasagna L (1995) Drug safety discontinuations in the United Kingdom, the United States, and Spain from 1974 through 1993: A regulatory perspective. *Clin Pharmacol Ther* 58(1):108–117.
8. Lin T, et al. (2009) A chemical platform for improved induction of human iPSCs. *Nat Methods* 6(11):805–808.
9. Polo JM, et al. (2010) Cell type of origin influences the molecular and functional properties of mouse induced pluripotent stem cells. *Nat Biotechnol* 28(8):848–855.
10. Takayama K, et al. (2013) Long-term self-renewal of human ES/iPS-derived hepatoblast-like cells on human laminin 111-coated dishes. *Stem Cell Reports* 1(4):322–335.
11. McDonald MG, Rettie AE (2007) Sequential metabolism and bioactivation of the hepatotoxin benzbromarone: Formation of glutathione adducts from a catechol intermediate. *Chem Res Toxicol* 20(12):1833–1842.
12. Kaufmann P, et al. (2005) Mechanisms of benzarone and benzbromarone-induced hepatic toxicity. *Hepatology* 41(4):925–935.
13. Ingelman-Sundberg M (2005) Genetic polymorphisms of cytochrome P450 2D6 (CYP2D6): Clinical consequences, evolutionary aspects and functional diversity. *Pharmacogenomics J* 5(1):6–13.
14. Spina E, et al. (1997) Relationship between plasma desipramine levels, CYP2D6 phenotype and clinical response to desipramine: A prospective study. *Eur J Clin Pharmacol* 51(5):395–398.
15. Nishimura K, et al. (2011) Development of defective and persistent Sendai virus vector: A unique gene delivery/expression system ideal for cell reprogramming. *J Biol Chem* 286(6):4760–4771.

THE JOURNAL OF BIOLOGICAL CHEMISTRY VOL. 289, NO. 34, pp. 23786–23795, August 22, 2014

Interferon-α Acts on the S/G_2/M Phases to Induce Apoptosis in the G_1 Phase of an IFNAR2-expressing Hepatocellular Carcinoma Cell Line*[S]

Received for publication, January 21, 2014, and in revised form, June 17, 2014 Published, JBC Papers in Press, July 10, 2014, DOI 10.1074/jbc.M114.551879

Sakae Maeda[‡§], Hiroshi Wada[§], Yoko Naito[‡], Hiroaki Nagano[§], Szandor Simmons[‡¶], Yoshinori Kagawa[‡§], Atsushi Naito[‡§], Junichi Kikuta[‡¶], Taeko Ishii[‡], Yoshito Tomimaru[§], Naoki Hama[§], Koichi Kawamoto[§], Shogo Kobayashi[§], Hidetoshi Eguchi[§], Koji Umeshita[§], Hideshi Ishii[§], Yuichiro Doki[§], Masaki Mori[§1], and Masaru Ishii[‡¶2]

From the Departments of [‡]Immunology and Cell Biology and [§]Gastroenterological Surgery, Graduate School of Medicine and Frontier Biosciences, Osaka University, 2-2 Yamada-oka, Suita, Osaka 565-0871, Japan and the [¶]Japan Science and Technology Agency, CREST, 5 Sanban-cho, Chiyoda-ku, Tokyo 102-0075, Japan

Background: The mode of action of interferon-α has been unknown.
Results: Its point of action in the cell cycle was analyzed by single cell tracking using time lapse confocal imaging.
Conclusion: Interferon-α activates p63 in S/G_2/M and induces apoptosis and cell cycle arrest in the subsequent G_1.
Significance: Tracking cell cycle progression is crucial for understanding the mechanisms of interferon-α.

Interferon-α (IFN-α) is used clinically to treat hepatocellular carcinoma (HCC), although the detailed therapeutic mechanisms remain elusive. In particular, IFN-α has long been implicated in control of the cell cycle, but its actual point of action has not been clarified. Here, using time lapse imaging analyses of the human HCC cell line HuH7 carrying a fluorescence ubiquitination-based cell cycle indicator (Fucci), we found that IFN-α induced cell cycle arrest in the G_0/G_1 phases, leading to apoptosis through an IFN-α type-2 receptor (IFNAR2)-dependent signaling pathway. Detailed analyses by time lapse imaging and biochemical assays demonstrated that the IFN-α/IFNAR2 axis sensitizes cells to apoptosis in the S/G_2/M phases in preparation for cell death in the G_0/G_1 phases. In summary, this study is the first to demonstrate the detailed mechanism of IFN-α as an anticancer drug, using Fucci-based time lapse imaging, which will be informative for treating HCC with IFN-α in clinical practice.

Hepatocellular carcinoma (HCC)[3] is one of the most common malignant diseases worldwide. HCC is commonly preceded by chronic inflammation such as that caused by hepatitis C virus (1). Interferons are secreted from hepatocytes as an immunological response to hepatitis C virus infection (2). Interferons not only trigger innate and adaptive immune responses but also regulate proliferation, differentiation, and apoptosis of different cell types, and they have therefore been used for clinical treatment of leukemia and other cancers (3).

Human interferons are classified into three major subtypes (types I–III). Among them, interferon-α (IFN-α) binds specifically to the heteromeric type I interferon receptor complex comprising interferon-α receptor-1 and -2 (IFNAR1 and IFNAR2), which utilize JAK tyrosine kinase and STAT transcription factors to activate interferon response genes (4). Phosphorylated STAT1 and STAT2 form a multimeric complex with IFN-regulatory factor 9 (IRF9), known as IFN-stimulated gene factor 3 (ISGF3), which then translocates to the nucleus and binds to IFN-stimulated response elements to initiate gene transcription (5, 6). It was previously reported that combinatorial treatment with IFN-α and 5-fluorouracil (5-FU), an anticancer agent, against advanced HCC results in an efficient clinical outcome (20.0% of patients showed a complete response, and 13.3% showed a partial response) (7). The therapeutic effects could be seen only in HCCs expressing high levels of IFNAR2, indicating the importance of the IFN-α/IFNAR2 axis (7, 8).

Aside from the accumulated evidence of its clinical utility, the actual therapeutic mechanisms remain obscure, although some previous reports have indicated the significance of cell cycle regulation in the anticancer action of the IFN-α/IFNAR2 axis. IFN-α was shown to induce G_1 arrest (9) and increase susceptibility to cytotoxic anticancer drugs (10), such as 5-FU, mainly targeting the S phase. However, these effects were evaluated based only on flow cytometry and remain controversial (11–13). Observation of apoptosis induction by IFN-α in living cells and monitoring of cell death at distinct cell cycle stages over time are essential to clarify the mechanisms of the cellular responses induced by IFN-α.

* This work was supported by Grants-in-Aid for Scientific Research on Innovative Areas 22113007; by Grant-in-Aid for Scientific Research (A) 25253070; by the FIRST Program from the Ministry of Education, Science, Sports, and Culture of Japan; by grants from the International Human Frontier Science Program (RGY0077/2011); and by grants from the Cell Science Research Foundation. This work was also supported by Japan Society for the Promotion of Science KAKENHI Grant 24791414.
[S] This article contains supplemental Videos 1–4.
[1] To whom correspondence may be addressed. Tel.: 81-6-6879-3258; Fax: 81-6-6879-3259; E-mail: mmori@gesrug.med.osaka-u.ac.jp.
[2] To whom correspondence may be addressed: Dept. of Immunology and Cell Biology, Graduate School of Medicine and Frontier Biosciences, Osaka University, 2-2 Yamada-oka, Suita, Osaka 565-0871, Japan. Tel.: 81-6-6879-3880; Fax: 81-6-6879-3889; E-mail: mishii@icb.med.osaka-u.ac.jp.
[3] The abbreviations used are: HCC, hepatocellular carcinoma; 5-FU, 5-fluorouracil; Fucci, fluorescence ubiquitination-based cell cycle indicator; IRES, intraribosomal entry site; qRT-PCR, quantitative real-time RT-PCR; qPCR, quantitative PCR; TA, transactivation; PUMA, p53 up-regulated modulator of apoptosis.

The fluorescence ubiquitination-based cell cycle indicator (Fucci) is a fluorescent probe that detects the various stages of the cell cycle in living cells (14). In this system, geminin, a nuclear protein enriched in the $S/G_2/M$ phases, and Cdt1, which is enriched in the G_0/G_1 phase, are marked by green and red fluorescent proteins, respectively.

In this study, we exploited these advanced imaging technologies to analyze the therapeutic mechanism of IFN-α against IFN-α-susceptible HCCs, particularly in association with the cell cycle.

EXPERIMENTAL PROCEDURES

Cell Lines and Reagents—The human HCC cell line HuH7 was obtained from the Japan Cancer Research Resources Bank (Tokyo, Japan). These cells were maintained in Dulbecco's modified Eagle's medium supplemented with 10% fetal bovine serum, 100 units/ml penicillin, and 100 mg/ml streptomycin at 37 °C in a humidified incubator with 5% CO_2 in air. Cells were treated with either purified human IFN-α (kindly provided by Otsuka Pharmaceutical Co., Tokyo, Japan) at final concentrations of 10–10,000 IU/ml or 5-FU (Wako Pure Chemical Industries, Osaka, Japan) at final concentrations of 10, 100, or 1000 μM. To synchronize the cell cycle of HuH7 cells, the cells were treated with aphidicolin (Calbiochem) at a final concentration of 1.6 μg/ml for 24 h.

TABLE 1
List of primer sequences used for RT-PCR analysis in this study

Primer	Sequence
GAPDH forward primer	5′-GTCGGAGTCAACGGATTTGGT-3′
GAPDH reverse primer	5′-GCCATGGGTGGAATCATATTGG-3′
IFNAR1 forward primer	5′-ATTTACACCATTTCGCAAAGCTC-3′
IFNAR1 reverse primer	5′-TCCAAAGCCCACATAACACTATC-3′
IFNAR2 forward primer	5′-GAAGGTGGTTAAGAACTGTGC-3′
IFNAR2 reverse primer	5′-CCCGCTGAATCCTTCTAGGACGG-3′
TAp63 forward primer	5′-GTCCCAGAGCACACAGACAA-3′
TAp63 reverse primer	5′-GAGGAGCCGTTCTGAATCTG-3′
ΔNp63 forward primer	5′-CTGGAAAACAATGCCCAGAC-3′
ΔNp63 reverse primer	5′-GGGTGATGGAGAGAGAGCAT-3′
p21 forward primer	5′-GACACCACTGGAGGGTGACT-3′
p21 reverse primer	5′-CAGGTCCACATGGTCTTCCT-3′
PUMA forward primer	5′-GCCAGATTTGTGAGACAAGAGG-3′
PUMA reverse primer	5′-CAGGCACCTAATTGGGCTC-3′

Generation of IFNAR2-expressing Fucci-introduced Cell Lines—Full-length cDNA of the human interferon-α/β receptor β-chain precursor (IFNAR2), obtained from Kazusa DNA Research Institute (Chiba, Japan), was inserted in front of the intraribosomal entry site (IRES) of the retroviral vector, pMX-IRES-Puro, using EcoRI sites to obtain pMX-IFNAR2. Replication-defective retroviruses were generated by transient transfection of pMX-IFNAR2 or pMX-IRES-Puro (control) into PLAT-A cells using FuGene 6 reagent (Promega, Tokyo, Japan) (15). HuH7 cells were transduced with the resulting retroviruses as described previously (16) and positively selected and expanded in the presence of 2 μg/ml puromycin. mAG-hGeminin mKO2-hCdt1 (kindly provided by Dr. Miyawaki, RIKEN-BSI, Japan) was cloned into the lentiviral vector CSII-EF-MCS (kindly provided by Dr. Miyoshi, RIKEN-BRC, Japan) and transfected into HEK293T cells with packaging plasmids (17). Lentiviral supernatant was used to transduce HuH7 cells. To select double-transduced cells, double-positive (Fucci green (mAG) and Fucci red (mKO2)) HuH7 cells were subsequently purified using a FACSAria cell sorter (BD Biosciences), as described below.

Quantitative Real-time RT-PCR and Immunoblot Analyses—Quantitative real-time RT-PCR (qRT-PCR), preparation of cell lysates, and immunoblot analyses were performed according to a previous report (18). All oligonucleotides used for qRT-PCR analyses were designed to amplify cDNA across exon-intron junctions, as described in Table 1. All data were normalized against internal GAPDH controls. Relative expression levels of IFNAR1 and IFNAR2 of WT controls were set as 1, and mRNA levels of mock and IFNAR2-expressing HuH7 samples were accordingly plotted as a -fold change. A full-length human p63 cDNA sequence, obtained from the Kazusa DNA Research Institute (Chiba, Japan), was transfected into HuH7 cells using FuGENE6 (Promega, Tokyo, Japan), according to the manufacturer's protocol. Cell lysates ware collected 1 day after transfection to perform qRT-PCR analyses.

To analyze activation of STAT1, -2, and -3, we performed immunoblot analyses using the primary antibodies described in Table 2. Mock control and IFNAR2-expressing cells were cultured in medium containing 10% FBS for 2 days and then in

TABLE 2
List of antibodies used for immunoblotting analysis in this study

Antibody	Source
Mouse anti-human IFNAR1 (H-11)	Santa Cruz Biotechnology
Rabbit anti-human IFNAR2	Otsuka Pharmaceutical
Rabbit anti-human STAT1 (CST 9172)	Cell Signaling Technology
Rabbit anti-human phospho-STAT1 (CST 9171)	Cell Signaling Technology
Rabbit anti-human STAT2 (CST 4441)	Cell Signaling Technology
Rabbit anti-human phospho-STAT2 (CST 4549)	Cell Signaling Technology
Rabbit anti-human STAT3 (CST 4904)	Cell Signaling Technology
Rabbit anti-human phospho-STAT3 (CST 9145)	Cell Signaling Technology
Mouse IgG-HRP conjugated anti-human actin	GenScript USA Inc.
Mouse anti-human p53 (DO-1)	Santa Cruz Biotechnology
Mouse anti-human p63 (4A4)	Santa Cruz Biotechnology
Mouse anti-human p21 (187)	Santa Cruz Biotechnology
Rabbit anti-human caspase-3 (CST 9662)	Cell Signaling Technology
Rabbit anti-human active caspase-3 (CST 9661)	Cell Signaling Technology
Rabbit anti-human caspase-7 antibody (CST 9492)	Cell Signaling Technology
Rabbit anti-human active caspase-7 antibody (CST 9492)	Cell Signaling Technology
Rabbit anti-human p38 (Poly 6224)	BioLegend
Rabbit anti-human phospho-p38 (CST 4631)	Cell Signaling Technology
HRP-labeled polyclonal secondary anti-rabbit (NA934V)	GE Healthcare
HRP-labeled anti-mouse-specific antibodies (NA931V)	GE Healthcare

FBS-free medium for 2 h. They were then incubated in medium with IFN-α (100 IU/ml) for 0–80 min, and the cells were lysed with mammalian lysis buffer (Promega, Tokyo, Japan). Cell lysates (10 μg of protein/lane) were loaded on 4–20% Mini-PROTEAN® TGX™ gels (Bio-Rad), separated by electrophoresis, and blotted onto a nitrocellulose membrane. The membrane was blocked in PVDF Blocking Reagent for Can Get Signal® (Toyobo, Osaka, Japan) for 1 h at room temperature and incubated with the specific antibodies in Can Get Signal® Immunoreaction Enhancer Solution 1™ (Toyobo, Osaka, Japan) overnight at 4 °C. After washing in 1× TBS-T, the membranes were incubated with HRP-labeled polyclonal secondary anti-rabbit (NA934V; GE Healthcare) or anti-mouse-specific antibodies (NA931V; GE Healthcare). Chemiluminescence was detected with an ECL Prime Kit (PerkinElmer Life Sciences) using an LAS4000 imaging system (GE Healthcare).

To analyze IFN-α/IFNAR2 signaling in G_0/G_1 or $S/G_2/M$ phases, IFNAR2-expressing Fucci-labeled HuH7 cells were treated with or without IFN-α (1,000 IU/ml) and sorted by FACS 24 h after treatment. Immunoblotting was performed as described above. The primary antibodies are listed in Table 2.

To deplete p63 expression, we performed RNAi with MISSION siRNA (Hs_TP63_6771 for TP63-specific and MISSION siRNA Universal Negative Control 1 for control; Sigma). RNA duplexes were transfected into IFNAR2-expressing HuH7 cells with RNAi MAX (Invitrogen) according to the manufacturer's instructions. After 24 h of transfection, cells were treated with 1,000 IU/ml IFN for 0, 24, or 48 h. qRT-PCR and immunoblot analyses were performed as described above (18).

Time Lapse Imaging—Cells ($1.5 \times 10^4/cm^2$) were grown overnight at 37 °C before imaging on a glass bottom dish in phenol red-free Dulbecco's modified Eagle's medium containing 10% FBS. Time lapse imaging was performed every 30 or 60 min with a confocal A1 microscope system (Nikon, Tokyo, Japan) equipped with a humidified imaging chamber (Nikon) at 37 °C, 5% CO_2 in air. Time lapse images were analyzed using Nikon NIS-Elements software (Nikon).

Cells were defined as apoptotic if they showed morphological changes, such as cell shrinkage and fragmentation into membrane-bound apoptotic bodies. The fluorescent signal detected in apoptotic cells was used to identify the cell cycle phases at which apoptosis occurred (*red*, G_0/G_1; *green*, $S/G_2/M$). To analyze the relationship between the cell cycle and apoptosis, each individual cell was tracked, and cell cycle changes and cell fate were monitored for 72 h. The frequency of cell death was calculated by dividing the initial total cell number in the visual field at $t = 0$ by the number of apoptotic cells for each cell cycle phase at the time of cell death ($t = 0$ until $t = 72$ h).

Flow Cytometry—To analyze the DNA content of Fucci-transfected HuH7 cells, we stained the cells with Hoechst 33342 (final concentration, 3.6 μg/ml; Invitrogen). After incubation for 30 min, cells were harvested and analyzed using a FACSCanto II flow cytometer (BD Biosciences). Both mKO2 and mAG were excited by a 488-nm laser, and Hoechst 33342 dye was excited by a 325-nm laser. Fluorescence signals were collected at 530 nm (530/28 BP) for mAG, at 575 nm (575/26 BP) for mKO2, and at 400 nm (380 LP) for Hoechst 33342 dye (14).

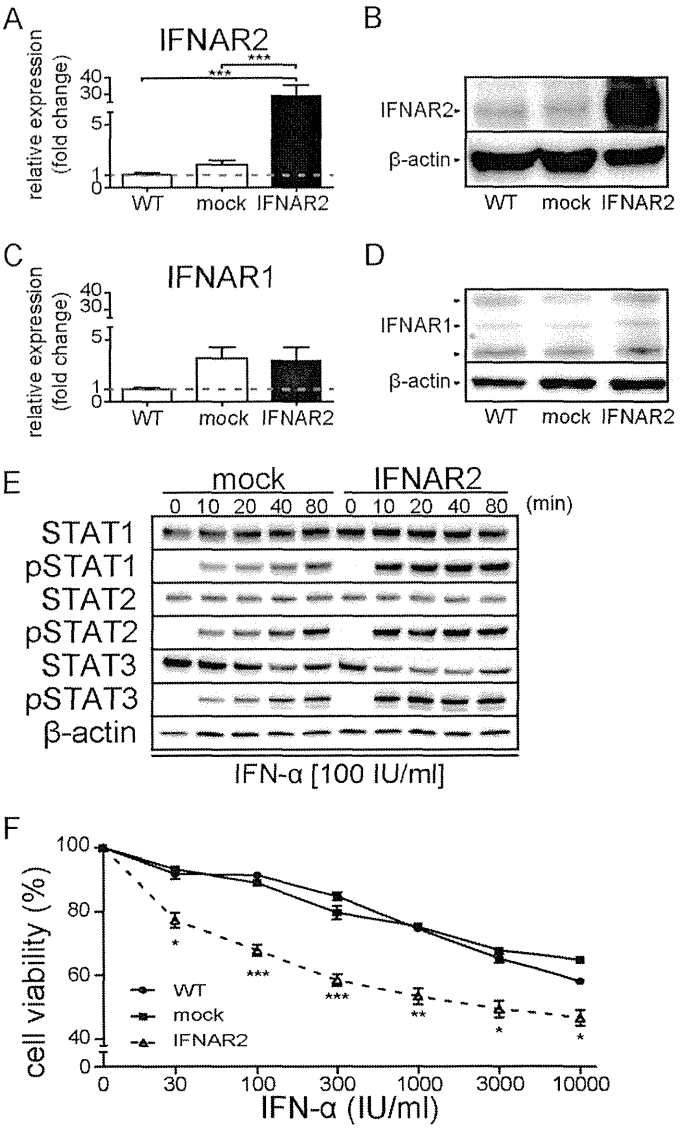

FIGURE 1. **Exogenous expression of IFNAR2 in HuH7 cells confers susceptibility to IFN-α treatment.** *A*, relative levels of IFNAR2 mRNA detected by qPCR in WT-, empty vector (mock)-, and IFNAR2-transfected HuH7 cells. Each *bar* represents the mean ± S.E. (*error bars*) of three individual experiments ($n = 3$ for each). ***, $p < 0.005$. *B*, Western blot detection of IFNAR2 protein from total cellular lysates of non-transfected (WT), empty vector transfected (mock), and IFNAR2-transfected HuH7 cells. *C*, relative amount of IFNAR1 mRNA detected by qPCR in WT and expressing empty vector (mock) or IFNAR2 HuH7 cells. Each bar represents the mean ± S.E. (*error bars*) of three individual experiments ($n = 3$ for each). *D*, Western blot detection of IFNAR1 protein from total cellular lysates of WT-, mock-, and IFNAR2-transfected HuH7 cells. *E*, Western blot detection of STAT1, -2, and -3 proteins and their phosphorylated forms from whole cell lysates of mock- or IFNAR2-transfected HuH7 cells. The lysates were collected at each time point after treatment with 100 IU/ml IFN-α. *F*, viability of HuH7 cells was examined by an MTT assay after treatment with different doses of IFN-α for 72 h. Cell viability is presented as the ratio of IFN-α-treated cells relative to untreated control cells. Statistical significance was determined between mock- and IFNAR2-expressing HuH7 cells at each IFN-α concentration, and the IC_{70} was determined for IFN-α-treated cells as follows: WT, 1,998.7 ± 200.5 IU/ml; mock, 2,389.1 ± 321.8 IU/ml; IFNAR2, 90.1 ± 36.1 IU/ml. Each *bar* represents the mean ± S.E. (*error bars*) of three individual experiments ($n = 3$ for each). *, $p < 0.05$; **, $p < 0.01$; ***, $p < 0.005$.

Preparative FACS sorting was performed using a FACSAria (BD Biosciences) cell sorter equipped with a 488-nm laser using 530/30BP or 585/42BP filters, respectively. The data were analyzed using FlowJo software (Tree Star, Inc., Ashland, OR).

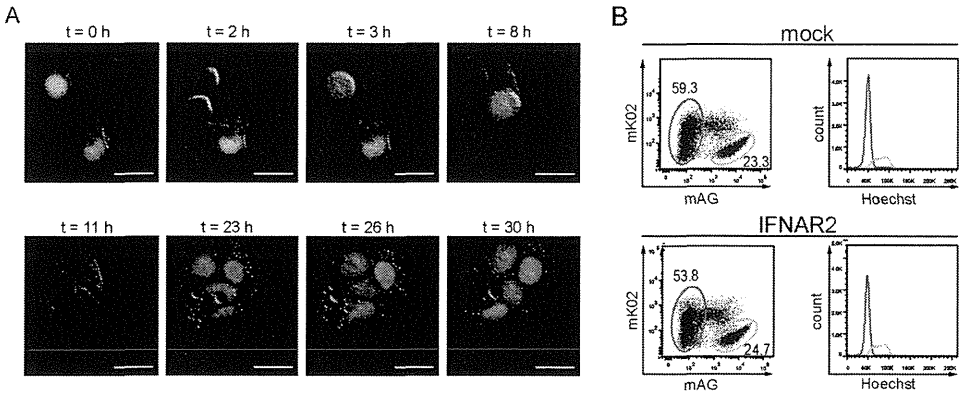

FIGURE 2. **Visualization of the cell cycle using the Fucci system.** *A*, representative images of cell cycle changes in IFNAR2-expressing Fucci-introduced HuH7 cells visualized by confocal time lapse imaging. *Red fluorescence* (mKO2-hCdt1) and *green fluorescence* (mAG-hGem) indicate G_0/G_1 and $S/G_2/M$ phases of the cell cycle, respectively. *B*, FACS analyses of mock- or IFNAR2-expressing Fucci-introduced HuH7 cells, identifying at least two distinct populations: mKO2-positive and mAG-negative (*red circled*) *versus* mKO2-negative and mAG-positive (*green circled*). The DNA content of each population was analyzed by staining with Hoechst 33342 dye (histograms). The *red* and *green lines* (in the *right panels*) represent histograms of the cells *circled* in *red* and *green* (in the *left panels*). These data confirmed that *red circled* cells (*i.e.* mKO2-positive G_1/G_0 cells) and *green circled* cells (*i.e.* mAG-positive $S/G_2/M$ cells) have 2N-DNA and 4N-DNA contents, respectively. *Numbers* indicate the frequencies (%) of living cells.

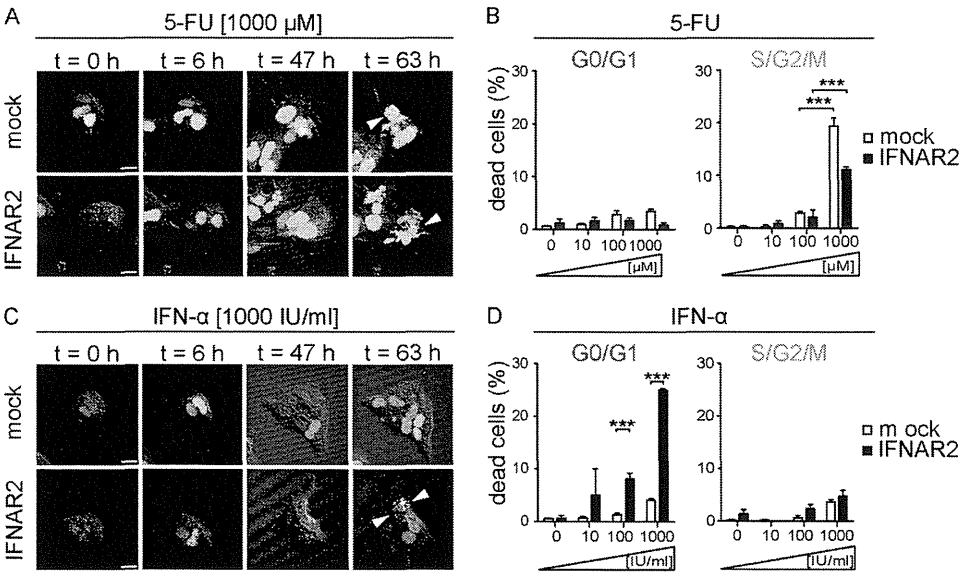

FIGURE 3. **Confocal time lapse imaging of apoptosis induction by 5-FU or IFN-α in IFNAR2-expressing Fucci-introduced HuH7 cells.** *A*, representative images from confocal time lapse imaging of Fucci-introduced IFNAR2-expressing HuH7 cells treated with 5-FU (1,000 μM) for 72 h. Red fluorescence (mKO2-hCdt1) and green fluorescence (mAG-hGeminin) represent the G_0/G_1 phases and $S/G_2/M$ phases of the cell cycle, respectively. *Arrowheads*, apoptotic cells. *Scale bar*, 10 μm. *B*, quantification of 5-FU-induced apoptosis at various phases of the cell cycle monitored by confocal time lapse imaging. Each *bar* represents the mean ± S.E. (*error bars*) of three individual experiments ($n = 3$). *C*, representative confocal time lapse images of Fucci-introduced IFNAR2-expressing HuH7 cells treated with IFN-α (1,000 IU/ml) for 72 h. *Arrowheads* indicate apoptotic cells. *Scale bar*, 10 μm. *D*, quantification of IFN-α-induced apoptosis at various phases of the cell cycle monitored by confocal time lapse imaging. Each *bar* represents the mean ± S.E. (*error bars*) of three individual experiments ($n = 3$).

3-(4,5-Dimethylthiazol-2-yl)-2,5-diphenyltetrazolium Bromide (MTT) Assay—The MTT assay was performed with the Cell Proliferation Kit 1 (Roche Applied Science) according to the manufacturer's protocol. In short, cells (1×10^3 cells/96-well dish) were grown overnight at 37 °C in a 96-well dish. Following treatment with or without IFN-α (30, 100, 300, 1,000, 3,000, and 10,000 IU/ml) for 72 h at 37 °C, cells were labeled with MTT-labeling reagent (MTT final concentration, 0.5 mg/ml; Roche Applied Science) for 4 h at 37 °C and subsequently solubilized with Solubilization Solution (Roche Applied Science) for 16 h at 37 °C. The absorbance was measured in a microplate reader (PowerScanHT; DS Pharma Biomedical, Osaka, Japan) at a wavelength of 550 nm with a 650-nm reference. The assays were carried out in 12 replicates at each IFN-α concentration in three individual experiments, and the results were plotted as a percentage of the absorbance relative to untreated controls. The concentration of IFN-α required to reduce the cell viability to 70% that of control cells (IC_{70}) was calculated from the spline curve generated using GraphPad Prism® software (GraphPad Software, Inc., La Jolla, CA).

Statistical Analyses—Differences between the control and treated groups were assessed by an unpaired Student's *t* test or Mann-Whitney *U* test and considered to be significant at $p < 0.05$ (*, $p < 0.05$; **, $p < 0.01$; ***, $p < 0.005$). Values are given as means ± S.E. Statistical analysis was performed using GraphPad Prism® software (version 5.0; GraphPad Software).

RESULTS

IFN-α Reduces the Viability of IFNAR2-expressing HCC Cells—To study the role of IFN-α in the induction of apoptosis of HCC cells, we transduced IFNAR2 into the human HCC cell

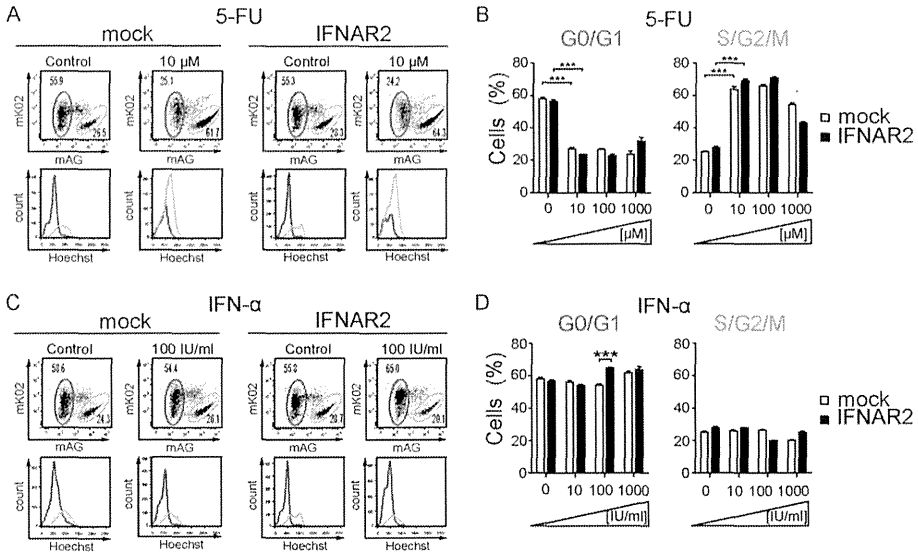

FIGURE 4. **Cell cycle analysis following 5-FU or IFN-α treatment using FACS.** *A* and *C*, representative dot plots from FACS analysis of mock- or IFNAR2-expressing Fucci-introduced HuH7 cells, 48 h after treatment with 10 μM 5-FU or 1,000 IU/ml IFN-α. The G_0/G_1 and $S/G_2/M$ populations were analyzed as described in the legend to Fig. 2. *B* and *D*, statistical analysis of four independent experiments 48 h after application of 5-FU (0, 10, 100, and 1,000 μM) or IFN-α (0, 10, 100, and 1,000 IU/ml). Bar graphs indicate the percentage of living cells in G_0/G_1 and $S/G_2/M$. Each *bar* represents the mean ± S.E. (*error bars*) of four independent experiments ($n = 4$). ***, $p < 0.005$.

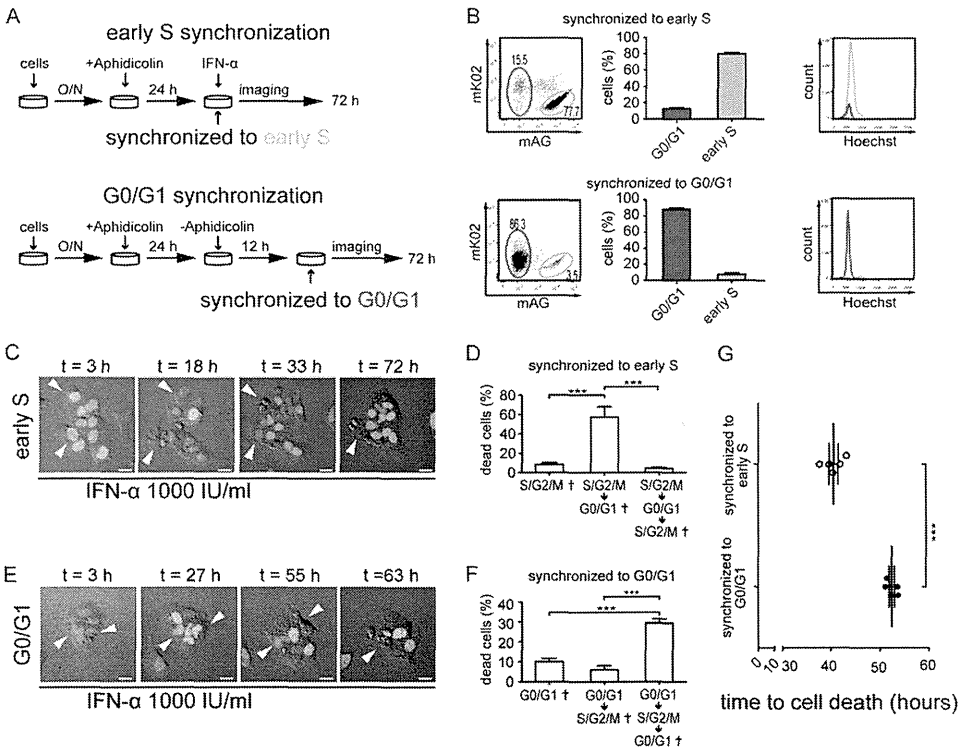

FIGURE 5. **Cell cycle synchronization revealed that IFN-α/IFNAR2 signaling acts on $S/G_2/M$ but induces apoptosis at the G_0/G_1 phases in HuH7 cells.** *A*, scheme of the protocol used to synchronize HuH7 cells to either early S phases (*top*) or to G_0/G_1 phases (*bottom*) by aphidicolin (1.6 μg/ml). *B*, confirmation of cell cycle synchronization upon aphidicolin treatment. IFNAR2-expressing Fucci-introduced HuH7 cells were analyzed by FACS. Cell cultures treated with aphidicolin for 24 h showed enrichment in the Fucci green population, whereas they were rather enriched in Fucci red when cultured for an additional 12 h in cells without aphidicolin. Bar graphs show the average values from five independent experiments. Cells were also analyzed by staining with Hoechst 33342 dye, representing the expected DNA content in each population. *C*, representative time lapse tracking images of early S-synchronized IFNAR2-expressing HuH7 cells treated with IFN-α (1,000 IU/ml) for 72 h. *Arrowheads*, apoptotic cells. *Scale bar*, 10 μm. *D*, frequency of cell death according to cell cycle phase. Relative numbers of cells that died in the first $S/G_2/M$ (*left*) and in the following G_1 (*middle*) and $S/G_2/M$ (*right*) phases are shown in the *columns*. Each *bar* represents the mean ± S.E. (*error bars*) of five individual experiments ($n = 5$). ***, $p < 0.005$. *E*, representative time lapse tracking images of G_0/G_1-synchronized IFNAR2-expressing HuH7 cells treated with IFN-α (1,000 IU/ml) for 72 h. *Arrowheads*, apoptotic cells. *Scale bar*, 10 μm. *F*, frequency of cell death in each cell cycle status. Relative numbers of cells that died in the first G_0/G_1 (*left*) and in the following $S/G_2/M$ (*middle*) and G_1 (*right*) phases are shown in the *columns*. Each *bar* represents the mean ± S.E. (*error bars*) of five individual experiments ($n = 5$). ***, $p < 0.005$. *G*, the time points of cell death induced by IFN-α after synchronized to early S phase or G_0/G_1 phase. Each *dot* shows the average of time points of cell death that were observed in time lapse tracking images of early S-synchronized or G_0/G_1-synchronized IFNAR2-expressing HuH7 cells treated with IFNA-α (1,000 IU/ml). Each *bar* represents the mean ± S.E. (*error bars*) of five individual experiments ($n = 5$). ***, $p < 0.005$.

line HuH7 with a constitutive retroviral expression vector for IFNAR2 (pMXs-IFNAR2) because the endogenous expression level of IFNAR2 in HuH7 cells is quite low (19). To confirm expression in HuH7 cells, we performed qPCR and immunoblot analyses. We obtained a HuH7 cell line expressing a higher level of IFNAR2, 30-fold higher in mRNA (Fig. 1*A*) and 9-fold higher in protein (Fig. 1*B*) than the mock control. Expression of IFNAR1 was also moderately increased in both the mock control and IFNAR2-expressing HuH7 cells (Fig. 1, *C* and *D*), possibly due to intrinsic cell responses against viral infection (20). To determine activation of the JAK/STAT signaling pathway upon IFN-α treatment of these cells, we performed immunoblot analyses to detect phosphorylation of STATs (STAT1, -2, and -3) (Fig. 1*E*). All STATs were phosphorylated in both the mock control and IFNAR2-expressing HuH7 cells, although the phosphorylation level was increased in IFNAR2-expressing HuH7 cells, indicating the function of exogenously expressed IFNAR2.

To confirm the responsiveness of these HuH7 cells to IFN-α treatment, we performed MTT assays (Fig. 1*F*). As expected, upon treatment with increasing concentrations of IFN-α, the viability of IFNAR2-expressing cells was significantly lower than that of WT and mock controls (Fig. 1*F*), indicating specific growth inhibition, such as apoptosis or cell cycle arrest induction through an IFN-α/IFNAR2 interaction. This result confirms that IFN-α negatively regulates cell viability in an IFNAR2-dependent manner and validates these IFNAR2-expressing HuH7 cells as a useful model with which to investigate the cellular responses of HCC to IFN-α therapy *in vitro*.

IFN-α Specifically Induces Apoptosis by an IFNAR2 Signaling Pathway at the G_0/G_1 Phases of the Cell Cycle—To examine the association between IFN-α action and cell cycle status, we introduced Fucci into the IFNAR2-expressing HuH7 cells and control (mock) HuH7 cells, both of which we have established (Fig. 1). Fucci-introduced IFNAR2-expressing HuH7 cells and mock controls allowed for tracking of individual cells over time and cell cycle changes during cell division by time lapse imaging using confocal microscopy (Fig. 2*A*). Furthermore, the DNA content (detected by a nuclear acid dye, Hoechst 33342) of Fucci-labeled HuH7 cells in the G_0/G_1 and $S/G_2/M$ phases varies according to the fluorescently indicated stages of the cell cycle in flow cytometric analyses (Fig. 2*B*), indicating the proper functioning of the Fucci system.

Concerning putative differential roles for IFN-α and 5-FU in effective clinical combination therapies for HCC, we performed *in vitro* time lapse imaging of Fucci-labeled IFNAR2-expressing HuH7 cells treated with IFN-α or 5-FU. Cells were defined as apoptotic if they showed morphological changes indicative of cell shrinkage and fragmentation into membrane-bound apoptotic bodies (21). First, we demonstrated that treatment with 5-FU, a nucleic acid analog that prevents cell division, led to accumulation of green ($S/G_2/M$) cells over time (Fig. 3*A* and supplemental Video 1) in a dose-dependent manner (Fig. 4, *A* and *B*). In addition, the cell death events (Fig. 3*A*, *arrowheads*) occurred preferentially in the green $S/G_2/M$ phases in both the control and IFNAR2-expressing HuH7 cells with comparable efficiency (Fig. 3*B*). These results are consistent with the conventional idea that nucleic acid analogs, such as 5-FU, block the

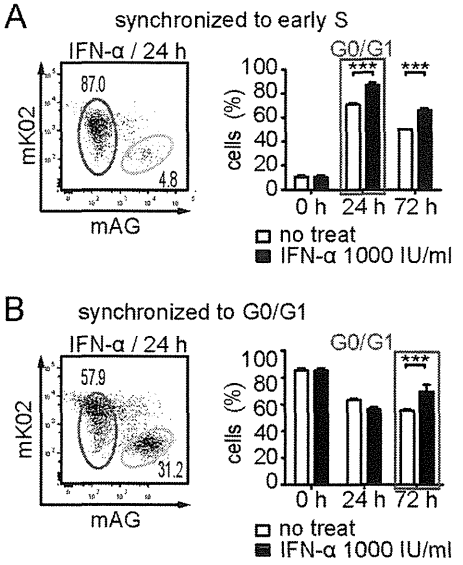

FIGURE 6. **FACS analysis after IFN-α treatment on cell cycle-synchronized cells.** *A*, time-dependent changes in cell cycle status of early S-synchronized cells. Cells were analyzed by FACS at the indicated time points with or without IFN-α treatment (1,000 IU/ml). Shown are a representative chart at 24 h (*left*) and the relative cell counts of the G_0/G_1 population (*right*). Each *bar* represents the mean ± S.E. (*error bars*) of three individual experiments ($n = 3$). ***, $p < 0.005$. *B*, time-dependent change in cell cycle status of G_0/G_1-synchronized cells with or without IFN-α treatment (1,000 IU/ml). A representative chart at 24 h (*left*) and the relative cell counts of the G_0/G_1 population (*right*). Each *bar* represents the mean ± S.E. (*error bars*) of three individual experiments ($n = 3$). ***, $p < 0.005$.

cell cycle at the S phase and exert cytotoxicity (22), and it was expected that this cytotoxic effect induced by 5-FU was not dependent on the expression of IFNAR2.

In contrast, IFN-α treatment resulted in an accumulation of red (G_0/G_1) IFNAR2-expressing HuH7 cells, and the results were not obvious in mock controls (Figs. 3*C* and 4 (*C* and *D*) and supplemental Video 2). Moreover, a high frequency of cell death in red (G_0/G_1) cells was also observed by time lapse imaging, albeit in only IFNAR2-expressing HuH7 cells (Fig. 3, *C* (*arrowheads*) and *D*). It should be noted that IFN-α treatment did not increase the rate of death of green ($S/G_2/M$) cells but resulted in an increased proportion of red (G_0/G_1) apoptotic cells at 100 or 1,000 IU/ml IFN-α, suggesting that IFN-α causes G_0/G_1 arrest.

These observations identified unique roles for IFN-α and 5-FU in inducing cell death at specific stages of the cell cycle. In addition, our data emphasize the importance of the IFN-α/IFNAR2 signaling pathway in regulating the efficiency of apoptosis induction at the G_0/G_1 phases of the cell cycle.

Cell Cycle Synchronization Revealed That IFN-α/IFNAR2 Signaling Acts on $S/G_2/M$ but Induces Apoptosis at the G_0/G_1 Phases in HuH7 Cells—To more precisely monitor the time course of the cell cycle-dependent IFN-α effect on IFNAR2-expressing HuH7 cells, we synchronized the cell cycle of HuH7 cells during G_0/G_1 to the early S boundary using aphidicolin, a reversible inhibitor of DNA polymerases (23). We were able to synchronize Fucci-transfected IFNAR2-expressing HuH7 cells to the early S phases (*green*) by the addition of aphidicolin for 24 h or to the G_0/G_1 phases (*red*) by removal of aphidicolin for 12 h (Fig. 5*A*). The relative populations of the cell cycle phases of the synchronized cells were evaluated by FACS, which indi-

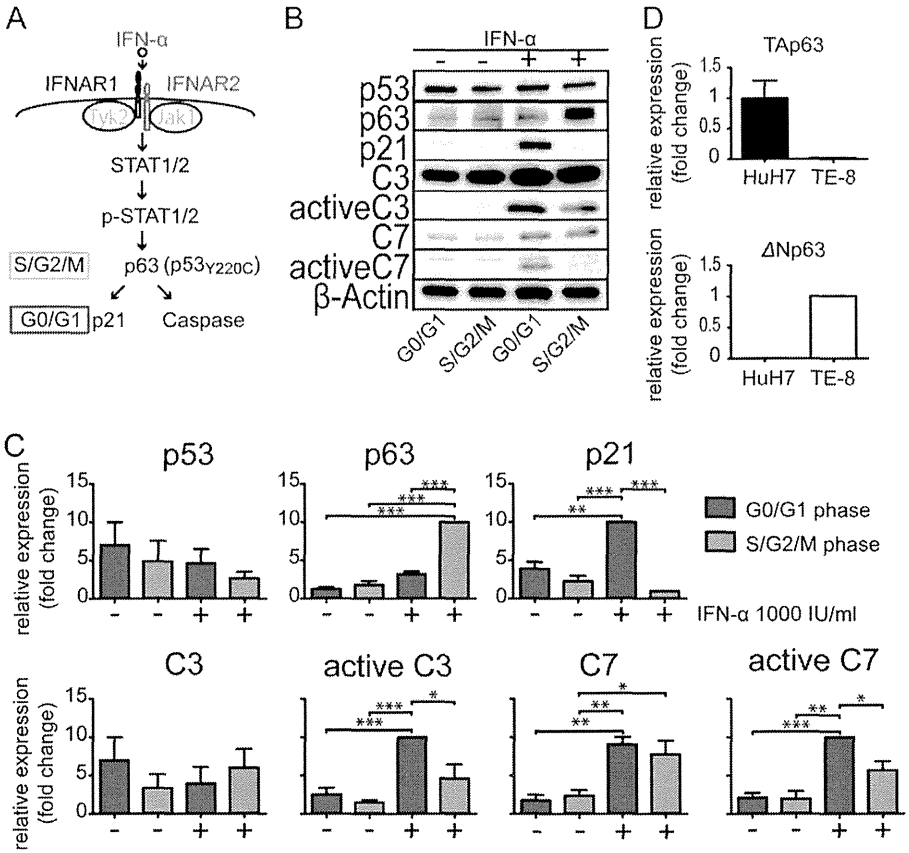

FIGURE 7. **Biochemical analyses of IFN-α/IFNAR2-induced signaling cascades in HuH7 cells.** *A*, schematic illustration of IFN-α-induced proapoptotic signaling, resulting in cell cycle arrest and apoptosis. *B*, expression of several critical signaling molecules activated by IFN-α, including p53, p63, p21, caspase-3 (*C3*), active caspase-3, caspase-7 (*C7*), active caspase-7, and β-actin (control). After culturing in the absence or presence of IFN-α (1000 IU/ml) for 24 h, IFNAR2-expressing Fucci-introduced HuH7 cells were sorted by FACS for the G_0/G_1 (mKO single positive) or $S/G_2/M$ (mAG single positive) and analyzed by Western blotting. *C*, densitometric analyses of Western blot data presented in Fig. 6*B*. The relative expression of each molecule was measured by ImageQuant TL version 7 (GE Healthcare). Each *bar* represents the mean ± S.E. (*error bars*) of three individual experiments ($n = 3$). *D*, relative mRNA expression levels of two isoforms of p63, TAp63 and ΔNp63, detected by qPCR in HuH7 and TE-8 cells. Each *bar* represents the mean ± S.E. (*error bars*) of three individual experiments ($n = 3$). *, $p < 0.05$; **, $p < 0.01$; ***, $p < 0.005$.

cated that 77.7 and 86.3% of cells were enriched to early S (*green*) or G_0/G_1 (*red*) by these methods, respectively (Fig. 5*B*).

Using this synchronization technique, we examined the effect of IFN-α exposure on the cell cycle of HuH7 cells. Most of the early S-synchronized cells (~57.1%) underwent apoptosis when they entered the next G_0/G_1 phase (Fig. 5, *C* (*arrowheads*) and *D*, and supplemental Video 3), suggesting that IFN-α-induced cell death occurs during mainly the G_0/G_1 phase. In contrast, a majority of the G_0/G_1-synchronized cells (~29.4%) died in the re-entered G_0/G_1 phase after going through the next $S/G_2/M$ phases (Fig. 5, *E* (*arrowheads*) and *F*, and supplemental Video 4). Concordantly, tracking of respective cell fates showed that cell deaths occurred faster in S phase-synchronized cells (40.6 ± 2.1 h) than in G_0/G_1-synchronized cells (52.4 ± 1.2 h) (Fig. 5*G*). We also checked the cell cycle status using FACS and found that IFN-α-induced accumulation of cells in the G_0/G_1 phase, which can be assumed to be a preapoptotic population, was detected earlier in the early S-synchronized cells (~24 h) (Fig. 6*A*), compared with the case with the G_0/G_1-synchronized cells (~72 h) (Fig. 6*B*). These results indicate that the $S/G_2/M$ phase is critical for receiving the "cell cycle arrest and death" signals from IFN-α, although the cells died mainly during the following G_0/G_1 phase.

Biochemical Analyses of IFN-α/IFNAR2- induced Signaling Cascades in HuH7 Cells—Finally, we assessed the molecular mechanisms underlying cell cycle-dependent IFN-α action. The interaction of IFN-α and IFNAR2 has been reported to activate the JAK/STAT signaling cascade, which is considered to be involved in G_1 arrest, leading to apoptosis (5) (Fig. 7*A*). To confirm the activation of this pathway, we performed immunoblotting for signaling components of the proapoptotic JAK/STAT pathways on IFNAR2-expressing Fucci-labeled HuH7 cells, which were used in the confocal time lapse imaging. Cells were treated or not treated with IFN-α for 24 h and separately collected for identification of G_0/G_1 or $S/G_2/M$ populations by cell sorting.

Expression of p53, which has been reported to play a central role in cell cycle arrest and apoptotic induction (6), was unaltered in HuH7 cells treated by IFN-α, irrespective of the cell cycle status (Fig. 7, *B* (*lane 1*) and *C*). This was probably because p53 in HuH7 cells carries a point mutation (Y220C) that renders it non-susceptible to IFN-α (24). Instead, we monitored the expression of p63, a molecule homologous to p53 (25, 26) and thus considered to play roles comparable with those of p53. We detected marked elevation of p63, especially during the $S/G_2/M$ phases (Fig. 7, *B* (*lane 2*) and *C*), suggesting that IFN-

α-induced apoptotic signals were activated preferentially in the $S/G_2/M$ phase. In the case of p63, there are two distinct promoters that result in two different types of proteins with opposing functions (*i.e.* p53-like proteins containing the transactivation (TA) domain (TAp63) and inhibitory proteins lacking the TA domain) (ΔNp63) (27). In our HuH7 cells, only TAp63 was confirmed to be expressed both at the mRNA (Fig. 7*D*) and protein levels (data not shown). In contrast, the increase in p21, which has been shown to be responsible for G_1 arrest (28), and the activation of caspase-3 and -7 could be preferentially detected in the G_0/G_1 phase (Fig. 7, *B* (*lanes 3–6*) and *C*), both of which have been shown to be inducible by p63 (29). These results were in agreement with the time lapse imaging results and suggest that IFN-α initiates its action during the $S/G_2/M$ phase and that cell cycle arrest and apoptosis occur in the subsequent G_0/G_1 phase. We detected significant up-regulation of STAT1/2 expression and phosphorylation upon stimulation with IFN-α in both the G_0/G_1 and $S/G_2/M$ phases (Fig. 8, *lanes 1–4*). In contrast, STAT3 was phosphorylated upon stimulation with IFN-α in both the G_0/G_1 and $S/G_2/M$ phases, and total expression of STAT3 was not affected by IFN-α treatment. IFN-α-activated JAKs are also known to regulate the activation of Vav or other guanine nucleotide exchange factors, resulting in the regulation of p38 mitogen-activated protein kinase (MAPK) (5). Both the expression and phosphorylation of p38 were not changed by these treatments (Fig. 8, *lanes 7* and *8*), suggesting that these pathways may not be dependent on the cell cycle. To examine whether p63 can induce cell cycle arrest and apoptosis in HuH7 cells, we examined the mRNA expression of p21 and p53 up-regulated modulator of apoptosis (PUMA) in p63 (TAp63)-transfected HuH7 cells. Upon overexpression of TAp63, both p21 and PUMA were significantly up-regulated ~4.0- and 3.7-fold, respectively (Fig. 9), indicating the potency of TAp63 for inducing proapoptotic signaling in HuH7 cells.

To examine whether the apoptosis induced by IFN-α was dependent on p63, we performed knockdown experiments of p63. Expression of p63 was confirmed to be reduced in p63-knockdown cells (Fig. 10*A*), and p63-knockdown cells showed less activation of caspase-3 and -7 (Fig. 10*B*). This result clearly suggests that p63 was critically involved in apoptosis induced by the IFN-α/IFNAR2 signaling pathway.

DISCUSSION

IFN-α has been used in the clinic to treat HCC, indicative of its therapeutic potential. However, its actual modes of action are less clear, precluding further development of this line of novel therapies (30). Flow cytometric analysis is commonly used for studying the cell cycle, although we did not observe cell death events with this conventional methodology. This study is the first to use confocal time lapse cell cycle imaging analyses with Fucci to visualize the specific relationship between cell cycle and cell death. The results demonstrated that IFN-α exerts its action on IFNAR2-expressing tumor cells by first sensitizing cells in the $S/G_2/M$ phases prior to inducing apoptosis in the G_1 phase. Combination therapy with IFN-α and 5-FU, commonly used clinically (30), can now be identified as an ideal regimen, because 5-FU is known to increase the $S/G_2/M$ population (see Fig. 4), which makes the tumor cells more susceptible to IFN-α. The present evidence provides clinicians with the rationale for use of this combination therapy and enables them to further improve the regimen based on its mode of action.

However, this study raises new questions. Among them is how the action of IFN-α is dependent on the cell cycle. Biochemical analyses indicated that "cell cycle-independent" activation of STAT1/2 signaling with up-regulation of p63, a proapoptotic signaling molecule, was observed predominantly in the $S/G_2/M$ phase. A promoter region of p63 reportedly contains putative binding motifs for E2F1, an E2F family transcription factor responsible for cell cycle regulation (31), although E2F1 may not bind to this motif by itself (32). Nevertheless, we can hypothesize that E2F1 or other cell cycle-dependent factors induce p63 expression if accompanied by STAT1 and -2 activation stimulated by IFN-α. On the other hand, it is also possible that the event of mitosis may be required for the induction of cell death by IFN-α. Further investigation is necessary to elucidate the whole picture of this intricate apoptotic signaling reg-

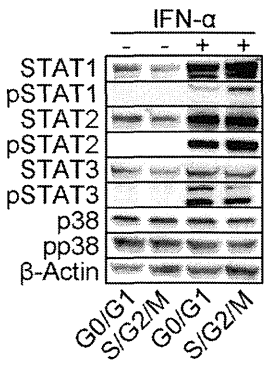

FIGURE 8. **Biochemical analyses of JAK/STAT and MAPK signaling.** The expression of several signaling molecules activated by IFN-α, including STAT1, phospho-STAT1 (*pSTAT1*), STAT2, phospho-STAT2 (*pSTAT2*), STAT3, phospho-STAT3 (*pSTAT3*), p38, phospho-p38 (*pp38*), and of β-actin (control) was analyzed by immunoblotting after culturing in the absence or presence of IFN-α (1,000 IU/ml) for 24 h. IFNAR2-expressing Fucci-introduced HuH7 cells were sorted by FACS for the G_0/G_1 (mKO single positive) or $S/G_2/M$ (mAG single positive) samples.

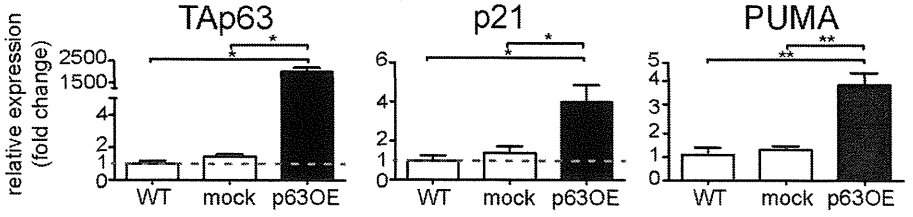

FIGURE 9. **Induction of proapoptotic factors, p21 and PUMA, by p63 in HuH7 cells.** Relative mRNA expression levels of TAp63, p21, and PUMA were detected by qPCR in wild-type HuH7 cells (*WT*) and in mock- or p63-overexpressing HuH7 cells (*p63OE*). Each *bar* represents the mean ± S.E. (*error bars*) of five individual experiments ($n = 5$ for each). *, $p < 0.05$; **, $p < 0.01$.

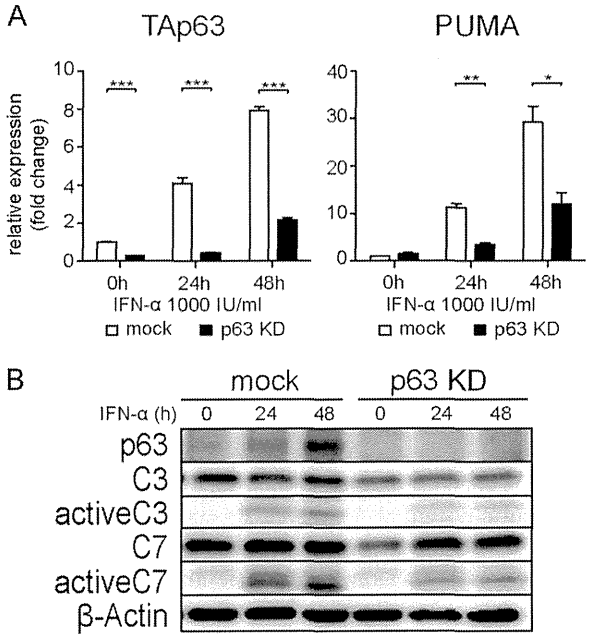

FIGURE 10. **Knockdown assay of p63 on IFNAR2-expressing HuH7 cells.** *A*, relative mRNA expression levels of TAp63 and PUMA in IFNAR2-expressing HuH7 cells after each time point of IFN-α (1,000 IU/ml) in p63 siRNA knockdown (*p63 KD*) and MISSION siRNA Universal Negative Control (*mock*). Each *bar* represents the mean ± S.E. (*error bars*) of triplicates. *B*, expression of apoptosis-related molecules in IFNAR2-expressing HuH7 cells measured by immunoblotting. p63-knockdown (*p63 KD*) or control cells (*mock*) were treated with IFN-α (1,000 IU/ml) for the indicated period of time. Protein levels of p63, caspase-3 (*C3*), active caspase-3, caspase-7 (*C7*), active caspase-7, and β-actin were measured by immunoblotting. *, $p < 0.05$; **, $p < 0.01$; ***, $p < 0.005$.

ulation associated with the cell cycle and controlled by therapeutic use of IFN-α.

Acknowledgments—We are grateful to Drs. A. Miyawaki and H. Miyoshi (RIKEN, Japan) for providing expression plasmids and advice and Drs. S. Seno and H. Matsuda (Osaka University) for image data analyses.

REFERENCES

1. Venook, A. P., Papandreou, C., Furuse, J., and de Guevara, L. L. (2010) The incidence and epidemiology of hepatocellular carcinoma: a global and regional perspective. *Oncologist* **15,** Suppl. 4, 5–13
2. Rehermann, B., and Nascimbeni, M. (2005) Immunology of hepatitis B virus and hepatitis C virus infection. *Nat. Rev. Immunol.* **5,** 215–229
3. Gutterman, J. U. (1994) Cytokine therapeutics: lessons from interferon α. *Proc. Natl. Acad. Sci. U.S.A.* **91,** 1198–1205
4. Pestka, S. (2007) The interferons: 50 years after their discovery, there is much more to learn. *J. Biol. Chem.* **282,** 20047–20051
5. Platanias, L. C. (2005) Mechanisms of type-I- and type-II-interferon-mediated signalling. *Nat. Rev. Immunol.* **5,** 375–386
6. Takaoka, A., Hayakawa, S., Yanai, H., Stoiber, D., Negishi, H., Kikuchi, H., Sasaki, S., Imai, K., Shibue, T., Honda, K., and Taniguchi, T. (2003) Integration of interferon-α/β signalling to p53 responses in tumour suppression and antiviral defence. *Nature* **424,** 516–523
7. Nagano, H., Miyamoto, A., Wada, H., Ota, H., Marubashi, S., Takeda, Y., Dono, K., Umeshita, K., Sakon, M., and Monden, M. (2007) Interferon-α and 5-fluorouracil combination therapy after palliative hepatic resection in patients with advanced hepatocellular carcinoma, portal venous tumor thrombus in the major trunk, and multiple nodules. *Cancer* **110,** 2493–2501
8. Ota, H., Nagano, H., Sakon, M., Eguchi, H., Kondo, M., Yamamoto, T., Nakamura, M., Damdinsuren, B., Wada, H., Marubashi, S., Miyamoto, A., Dono, K., Umeshita, K., Nakamori, S., Wakasa, K., and Monden, M. (2005) Treatment of hepatocellular carcinoma with major portal vein thrombosis by combined therapy with subcutaneous interferon-α and intra-arterial 5-fluorouracil: role of type 1 interferon receptor expression. *Br. J. Cancer* **93,** 557–564
9. Sangfelt, O., Erickson, S., and Grander, D. (2000) Mechanisms of interferon-induced cell cycle arrest. *Front. Biosci.* **5,** D479–D487
10. Kondo, M., Nagano, H., Wada, H., Damdinsuren, B., Yamamoto, H., Hiraoka, N., Eguchi, H., Miyamoto, A., Yamamoto, T., Ota, H., Nakamura, M., Marubashi, S., Dono, K., Umeshita, K., Nakamori, S., Sakon, M., and Monden, M. (2005) Combination of IFN-α and 5-fluorouracil induces apoptosis through IFN-α/β receptor in human hepatocellular carcinoma cells. *Clin. Cancer Res.* **11,** 1277–1286
11. Yano, H., Yanai, Y., Momosaki, S., Ogasawara, S., Akiba, J., Kojiro, S., Moriya, F., Fukahori, S., Kurimoto, M., and Kojiro, M. (2006) Growth inhibitory effects of interferon-α subtypes vary according to human liver cancer cell lines. *J. Gastroenterol. Hepatol.* **21,** 1720–1725
12. Sangfelt, O., Erickson, S., Castro, J., Heiden, T., Einhorn, S., and Grandér, D. (1997) Induction of apoptosis and inhibition of cell growth are independent responses to interferon-α in hematopoietic cell lines. *Cell Growth Differ.* **8,** 343–352
13. Murphy, D., Detjen, K. M., Welzel, M., Wiedenmann, B., and Rosewicz, S. (2001) Interferon-α delays S-phase progression in human hepatocellular carcinoma cells via inhibition of specific cyclin-dependent kinases. *Hepatology* **33,** 346–356
14. Sakaue-Sawano, A., Kurokawa, H., Morimura, T., Hanyu, A., Hama, H., Osawa, H., Kashiwagi, S., Fukami, K., Miyata, T., Miyoshi, H., Imamura, T., Ogawa, M., Masai, H., and Miyawaki, A. (2008) Visualizing spatiotemporal dynamics of multicellular cell-cycle progression. *Cell* **132,** 487–498
15. Morita, S., Kojima, T., and Kitamura, T. (2000) Plat-E: an efficient and stable system for transient packaging of retroviruses. *Gene Ther.* **7,** 1063–1066
16. Nishikawa, K., Nakashima, T., Hayashi, M., Fukunaga, T., Kato, S., Kodama, T., Takahashi, S., Calame, K., and Takayanagi, H. (2010) Blimp1-mediated repression of negative regulators is required for osteoclast differentiation. *Proc. Natl. Acad. Sci. U.S.A.* **107,** 3117–3122
17. Copeland, N. G., Gilbert, D. J., Schindler, C., Zhong, Z., Wen, Z., Darnell, J. E., Jr., Mui, A. L., Miyajima, A., Quelle, F. W., and Ihle, J. N. (1995) Distribution of the mammalian Stat gene family in mouse chromosomes. *Genomics* **29,** 225–228
18. Quelle, F. W., Thierfelder, W., Witthuhn, B. A., Tang, B., Cohen, S., and Ihle, J. N. (1995) Phosphorylation and activation of the DNA binding activity of purified Stat1 by the Janus protein-tyrosine kinases and the epidermal growth factor receptor. *J. Biol. Chem.* **270,** 20775–20780
19. Damdinsuren, B., Nagano, H., Wada, H., Noda, T., Natsag, J., Marubashi, S., Miyamoto, A., Takeda, Y., Umeshita, K., Doki, Y., Dono, K., and Monden, M. (2007) Interferon α receptors are important for antiproliferative effect of interferon-α against human hepatocellular carcinoma cells. *Hepatol. Res.* **37,** 77–83
20. Barchet, W., Cella, M., Odermatt, B., Asselin-Paturel, C., Colonna, M., and Kalinke, U. (2002) Virus-induced interferon α production by a dendritic cell subset in the absence of feedback signaling *in vivo*. *J. Exp. Med.* **195,** 507–516
21. Taylor, R. C., Cullen, S. P., and Martin, S. J. (2008) Apoptosis: controlled demolition at the cellular level. *Nat. Rev. Mol. Cell Biol.* **9,** 231–241
22. Shah, M. A., and Schwartz, G. K. (2001) Cell cycle-mediated drug resistance: an emerging concept in cancer therapy. *Clin. Cancer Res.* **7,** 2168–2181
23. Huberman, J. A. (1981) New views of the biochemistry of eucaryotic DNA replication revealed by aphidicolin, an unusual inhibitor of DNA polymerase α. *Cell* **23,** 647–648
24. Cagatay, T., and Ozturk, M. (2002) P53 mutation as a source of aberrant β-catenin accumulation in cancer cells. *Oncogene* **21,** 7971–7980
25. Yoshikawa, H., Nagashima, M., Khan, M. A., McMenamin, M. G., Hagiwara, K., and Harris, C. C. (1999) Mutational analysis of p73 and p53 in human cancer cell lines. *Oncogene* **18,** 3415–3421
26. Hagiwara, K., McMenamin, M. G., Miura, K., and Harris, C. C. (1999)

Mutational analysis of the p63/p73L/p51/p40/CUSP/KET gene in human cancer cell lines using intronic primers. *Cancer Res.* **59,** 4165–4169

27. Gressner, O., Schilling, T., Lorenz, K., Schulze Schleithoff, E., Koch, A., Schulze-Bergkamen, H., Lena, A. M., Candi, E., Terrinoni, A., Catani, M. V., Oren, M., Melino, G., Krammer, P. H., Stremmel, W., and Muller, M. (2005) TAp63α induces apoptosis by activating signaling via death receptors and mitochondria. *EMBO J.* **24,** 2458–2471
28. Deng, C., Zhang, P., Harper, J. W., Elledge, S. J., and Leder, P. (1995) Mice lacking p21CIP1/WAF1 undergo normal development, but are defective in G_1 checkpoint control. *Cell* **82,** 675–684
29. Dohn, M., Zhang, S., and Chen, X. (2001) p63α and ΔNp63α can induce cell cycle arrest and apoptosis and differentially regulate p53 target genes. *Oncogene* **20,** 3193–3205
30. Nagano, H., Wada, H., Kobayashi, S., Marubashi, S., Eguchi, H., Tanemura, M., Tomimaru, Y., Osuga, K., Umeshita, K., Doki, Y., and Mori, M. (2011) Long-term outcome of combined interferon-α and 5-fluorouracil treatment for advanced hepatocellular carcinoma with major portal vein thrombosis. *Oncology* **80,** 63–69
31. Waltermann, A., Kartasheva, N. N., and Dobbelstein, M. (2003) Differential regulation of p63 and p73 expression. *Oncogene* **22,** 5686–5693
32. Fogal, V., Hsieh, J. K., Royer, C., Zhong, S., and Lu, X. (2005) Cell cycle-dependent nuclear retention of p53 by E2F1 requires phosphorylation of p53 at Ser^{315}. *EMBO J.* **24,** 2768–2782

Int. J. Mol. Sci. **2015**, *16*, 3307-3322; doi:10.3390/ijms16023307

OPEN ACCESS
International Journal of
Molecular Sciences
ISSN 1422-0067
www.mdpi.com/journal/ijms

Review

Significant Roles of Regulatory T Cells and Myeloid Derived Suppressor Cells in Hepatitis B Virus Persistent Infection and Hepatitis B Virus-Related HCCs

Yasuteru Kondo * and Tooru Shimosegawa

Division of Gastroenterology, Tohoku University Graduate School of Medicine 1-1 Seiryo, Aoba, Sendai City, Miyagi 980-8574, Japan; E-Mail: tshimosegawa@int3.med.tohoku.ac.jp

* Author to whom correspondence should be addressed; E-Mail: yasuteru@ebony.plala.or.jp; Tel.: +81-22-717-7171; Fax: +81-22-717-7177.

Academic Editor: Tatsuo Kanda

Received: 5 December 2014 / Accepted: 28 January 2015 / Published: 3 February 2015

Abstract: The adaptive immune system, including type1 helper T cells (Th1 cells), cytotoxic T lymphocytes (CTLs), and dendritic cells (DCs), plays an important role in the control of hepatitis B virus (HBV). On the other hand, regulatory T cells (Tregs) and myeloid derived suppressor cells (MDSCs) suppress the immune reaction in HBV and hepatocellular carcinoma (HCC). Excessive activation of immune suppressive cells could contribute to the persistent infection of HBV and the progression of HCC. The frequency and/or function of Tregs could affect the natural course in chronic hepatitis B patients and the treatment response. In addition to the suppressive function of MDSCs, MDSCs could affect the induction and function of Tregs. Therefore, we should understand in detail the mechanism by which Tregs and MDSCs are induced to control HBV persistent infection and HBV-related HCC. Immune suppressive cells, including Tregs and MDSCs, contribute to the difficulty in inducing an effective immune response for HBV persistent infection and HBV-related HCC. In this review, we focus on the Tregs and MDSCs that could be potential targets for immune therapy of chronic hepatitis B and HBV-related HCC.

Keywords: regulatory T cells (Tregs); myeloid derived suppressor cells (MDSCs); hepatitis B virus (HBV); hepatocellular carcinoma (HCC)

1. Introduction

Hepatitis B virus (HBV) is a noncytopathic DNA virus that causes chronic hepatitis and hepatocellular carcinoma (HCC) as well as acute hepatitis [1]. HBV infects more than 400 million people worldwide. HBV has six different genotypes [2,3]. The progression of liver fibrosis and HCC could vary among various HBV genotypes [3,4].

It has been reported that the innate immune system, including intra-hepatocyte reactions [5,6], natural killer cells (NK cells), natural killer T cells (NK-T cells), and monocytes, could contribute to the immunopathogenesis of HBV infection [7–12]. However, the adaptive immune system, including type 1 helper T cells (Th1 cells), cytotoxic T lymphocytes (CTLs), and dendritic cells (DCs), plays an important role in the control of HBV [13–18]. On the other hand, $CD4^+CD25^+FOXP3^+$ regulatory T cells (Tregs) and myeloid derived suppressor cells (MDSCs) suppress the immune reactions to HBV and HCC [19–24]. The excessive activation of immune suppressive cells could contribute to the persistent infection of HBV and the progression of HCC. Tregs constitutively express CD25 in the physiological state [25]. In humans, this population, as defined by $CD4^+CD25^+FOXP3^+$ T cells, constitutes 5% to 10% of peripheral $CD4^+$ T lymphocytes and has a broad repertoire that recognizes various self and non-self antigens [26–28]. Various kinds of immune suppressing mechanisms-induced by Tregs have been reported [28]. The important mechanisms are cell-to-cell contact and secretion of immune-suppressive cytokines including transforming growth factor-β (TGF-β) and IL10 [19,23,28]. An emerging cell population of interest, MDSCs, could contribute to immune suppression. MDSCs are a heterogeneous population of immature myeloid cells, originally shown to accumulate at the sites of tumors. MDSCs have been well described in various severe human diseases such as cancer, autoimmune diseases, and bacterial infections [19,29,30]. In mouse, populations of MDSCs have been divided into two groups: polymorphonuclear MDSCs (PMN-MDSC), described as $CD11b^+Gr\text{-}1^{high}Ly6^+Ly6C^{low/int}$ cells, and mononuclear MDSCs (Mo-MDSC), described as $CD11b^+Gr\text{-}1^{int}Ly6G^-Ly6C^{high}$ cells [31,32]. On the other hand, in human, the phenotypic markers of MDSCs are less clear. MDSCs have been described as $CD33^+CD11b^+HLA\text{-}DR^{low/-}$ in a human cancer model [32] (Table 1). It has been reported that MDSCs could contribute to persistent infection of HBV and HCC [19,20,30,33–38] (Table 1). In addition to HBV and HCC, MDSCs could contribute to persistent infection of HCV [39,40]. HCV core-treated $CD33^+$ cells exhibit a $CD14^+CD11b^{+/low}$ $HLA\text{-}DR^{-/low}$ phenotype with up-regulated reactive oxygen species (ROS) production [39]. Moreover, the frequency of MDSCs increases and correlates with HCV-RNA loads in chronic hepatitis C (CH-C) patients [40]. MDSCs could suppress the T cell response by way of numerous mechanisms including the expression of inhibitory cell surface molecules, the production of immune suppressive cytokines, the metabolism of arginine through activation of arginase-1, production of nitric oxide, and the up-regulation of reactive oxygen species. Moreover, an interaction between MDSCs and Tregs has been reported [20,31,32,41–43]. MDSCs and Tregs could contribute to not only HCC but also various kinds of cancers [43–63] (Table 2). Many groups reported the frequency of MDSCs, and Tregs could be useful prognostic biomarkers. Moreover, some reports indicated the possibility of modifying the function of MDSCs and Tregs to improve the immune reaction to cancers by using CTLA-4 antibody, PD-L1 antibody, anti-miR214, c-kit antibody and sunitinib, *etc.* (Table 2).

Table 1. Association between MDSCs and HBV or HCC.

Species	MDSCs Phenotype	Diseases or Models of Diseases	Functions and Findings	References
Human	Lin-HLA-DR-$CD11b^{+}CD33^{+}$	HBV	MDSCs might be involved in HBeAg immune tolerance	Lu *et al.* [30]
Mouse	$CD11b^{+}Gr1^{+}$	HBV (mouse model)	gammadelta T Cells drive MDSCs–mediated CD8+ T Cell exhaustion	Kong *et al.* [33]
Mouse	$CD11b^{+}Gr1^{+}$	HBV (mouse model)	In HBV TM, the frequencies of liver MDSCs were about twice those of normal mice liver	Chen *et al.* [34]
Human	$CD34^{+}CD14^{-}$HLA-$DR^{-}CD11b^{+}$	HBV vaccination in HIV patients	High frequency of MDSCs contribute to week 16 HBV vaccine response	Anthony *et al.* [35]
Human	$CD14^{+}$HLA-$DR^{-/low}$	HCC	MDSCs induces CD4+CD25+Foxp3+ T Cells Frequency of CD14+ HLA-DR-/low cells Is Increased in PBMC and tumor of HCC patients	Hoechest *et al.* [19]
Human	$CD14^{+}$HLA-$DR^{-/low}$	HCC	MDSCs inhibit NK cells in HCC patients via the NKp30 receptor	Hoechest *et al.* [36]
Human	$CD14^{-}$HLA-$DR^{-}CD11b^{+}CD33^{+}$	HCC	Elevated numbers of MDSC in HCC patients Over-production of inhibitory cytokines such as IL10 and TGF-β	Kalathil *et al.* [20]
Mouse	$Gr^{+}CD11b^{+}$	HCC mouse model	An accumulation of MDSC is found in various mice models with HCC	Kapanadze *et al.* [37]
Mouse	$Gr^{+}CD11b^{int}$	HCC mouse model	Tumors produce IL-6 and VEGF and induced iMC (CD11b1Gr-1int)	Shmidl *et al.* [38]

Table 2. Association of Tregs and MDSCs and other cancers except for HCC.

Cancer	Immune Suppressive Cells		Treatments, Future Treatments or Other Uses	References
	Tregs	MDSCs		
Large B cell lymphoma	○		prognostic biomarker	Ahearne *et al.* [44]
Non-Hodgkin Lymphoma	○		prognostic biomarker	Pinheiro *et al.* [45]
Myeloma	○		CTLA-4 antibody	Braga *et al.* [46]
	○	○	High-dose IL2 followed by Sorafenib	Monk *et al.* [47]
		○	Adjuvant GM-CSF	Daud *et al.* [48]
	○	○	prognostic marker	Brimnes *et al.* [49]
Ovarian Cancer	○		prognostic biomarker	Brtnicky *et al.* [50]
Mouse model (liver metastasis model)		○	Anti-PD-L1 antibody	Ilkovitch *et al.* [51]
Esophageal Cancer	○		Down-regulation of B7-H1 expression	Chen *et al.* [52]